AD_____
(Leave blank)

Award Number:
W81XWH-10-1-0115

TITLE:
Photodynamic Molecular Beacons: An Image-Guided Therapeutic Approach to Breast Cancer Vertebral Metastases

PRINCIPAL INVESTIGATOR:
Tracy Liu

CONTRACTING ORGANIZATION:
University Health Network
Toronto, ON, Canada
M5G 2C4

REPORT DATE:
March 2011

TYPE OF REPORT:
Annual Summary

PREPARED FOR: U.S. Army Medical Research and Materiel Command
Fort Detrick, Maryland 21702-5012

DISTRIBUTION STATEMENT: (Check one)

✓ Approved for public release; distribution unlimited

REPORT DOCUMENTATION PAGE

Form Approved
OMB No. 0704-0188

1. REPORT DATE	2. REPORT TYPE	3. DATES COVERED
14-MAR-2011	Annual Summary	15 FEB 2010 - 14 FEB 2011

4. TITLE AND SUBTITLE
Photodynamic Molecular Beacons: An Image-Guided Therapeutic Approach to Breast Cancer Vertebral Metastases

5a. CONTRACT NUMBER
W81XWH-10-1-0115

5b. GRANT NUMBER

5c. PROGRAM ELEMENT NUMBER

6. AUTHOR(S)

Tracy Liu

Email: tliu@uhnres.utoronto.ca

5d. PROJECT NUMBER

5e. TASK NUMBER

5f. WORK UNIT NUMBER

7. PERFORMING ORGANIZATION NAME(S) AND ADDRESS(ES)

University Health Network
200 Elizabeth Street
Toronto, ON, Canada M5G 2C4

8. PERFORMING ORGANIZATION REPORT NUMBER

9. SPONSORING / MONITORING AGENCY NAME(S) AND ADDRESS(ES)
U.S. Army Medical Research and Materiel Command
Fort Detrick, Maryland 21702-5012

10. SPONSOR/MONITOR'S ACRONYM(S)

11. SPONSOR/MONITOR'S REPORT NUMBER(S)

12. DISTRIBUTION / AVAILABILITY STATEMENT
Approved for Public Release; Distribution Unlimited

13. SUPPLEMENTARY NOTES

14. ABSTRACT

The vertebral column is the most common site of breast cancer metastases, where overexpression of matrix metalloproteinases (MMPs) promotes the spread of cancer. Current therapies for managing vertebral metastases have significant limitations due to high associated risk of spinal cord damage. An attractive alternative is photodynamic therapy (PDT) providing non-invasive and site-selective treatment. However, current photosensitizers are limited by their non-specific accumulation. Photodynamic molecular beacons (PPMMPB), activated by MMPs, offer another level of PDT selectivity and image-guidance preserving criticial tissues, specifically the spinal cord. In vitro studies confirm the specific activation of PPMMPB in MT-1 cells. In vivo experiments demonstrate specific activation of PPMMPB in MT-1 xenografts, using systemic and intratumoral injections. Using a clinically-relevant metastatic model, fluorescent imaging confirmed the specific activation of PPMMPB by vertebral metastases. As a first step, we validate that the metastasis-selective mechanism of PPMMPBs can specifically image breast cancer vertebral metastases, thereby differentiating tumor and healthy tissue. Preliminary PPMMPB - PDT results demonstrate the specific PDT induced destruction of vertebral metastases while the spinal cord is left undamaged.

15. SUBJECT TERMS
Breast Cancer, Vertebral Metastases, Photodynamic Therapy, Protease Activatable Beacons, Matrix Metalloproteinase, Optical Imaging

16. SECURITY CLASSIFICATION OF:			17. LIMITATION OF ABSTRACT	18. NUMBER OF PAGES	19a. NAME OF RESPONSIBLE PERSON
a. REPORT	b. ABSTRACT	c. THIS PAGE			USAMRMC
U	U	U	UU	53	19b. TELEPHONE NUMBER *(include area code)*

Standard Form 298 (Rev. 8-98)
Prescribed by ANSI Std. Z39.18

Table of Contents

Page

Introduction:

Breast cancer is a leading killer in North America. Approximately 85% of breast cancer patients with metastatic disease will develop bone metastases, in which the vertebral column is the most common site for metastatic formation.(*1, 2*) Breast cancer metastasis disrupts the dynamic balance between bone resorption by osteoclasts and bone formation by osteoblasts, inducing a vicious cycle whereby tumor cells reprogram osteoclasts, leading to osteolysis and promotion of tumor growth.(*1, 3*) Matrix metalloproteinases (MMPs) are a family of structurally-related, zinc-dependent endopeptidases implicated in the invasion and metastasis of cancer.(*4-7*) The upregulation of MMPs is critically involved in the destruction of the delicate balance between bone formation and degradation, reducing bone integrity (Fig. 1).(*1, 3*) Hence, MMPs not only aid the spread of tumor cells to distant sites, but are also involved in the local dissolution of the vertebral body and promote tumor progression within the vertebrae. Patients with spinal metastases have a high risk of spinal cord compression, resulting in motor dysfunction, neurological compromise and an overall poor prognosis.(*1, 3*) The associated 5-year survival rate in patients with spinal metastases is below 20% compared to a 5-year survival rate over 85% in patients with early stage breast cancer.(*8*) Regardless of the symptoms, all patients suffering from spinal metastases experience a substantial decrease in their quality of life. Surgery and radiation therapy are the main treatment options for these patients. Surgical treatments, however, carry a high risk of morbidity due to the proximity of the spinal cord, while radiation therapy is limited to a level far below the optimal therapeutic dose because of the low tolerance of the spinal cord.(*9*) Clinical studies of radiotherapy have reported recurrence of symptoms, and pain relief is not experienced until at least 3 months after treatment.(*10*) Lastly, although pain relief and, in part, tumor regression are addressed by radiation treatment, spinal instability is not. Therein lies the need for improved therapies that specifically targets metastatic tumor cells while preserving the spinal cord to address pain relief, tumor regression and mechanical instability of the spine. PDT is an approved cancer treatment modality that destroys target cells when light activates a non-toxic photosensitizer (PS) to generate cytotoxic excited-state (singlet) oxygen.(*11-13*) It has several potential advantages over current cancer treatments due to its minimally-invasive nature, selectivity, ability to treat patients with repeated doses without initiating resistance or exceeding total-dose limitations, fast healing that results in little or no scarring, the ability to administer in an outpatient setting, minimal associated side effects and lack of contraindication with other modalities.(*11-13*) PDT has shown promising reports for destroying spinal metastases, particularly to debulk lesions as an adjuvant to vertebroplasty or kyphoplasty in order to mechanically stabilize weak or fractured vertebrae:(*14-19*) These surgical procedures involve injection of a plastic compound or placement of an inflatable balloon into the vertebral body, which is often limited by the space-occupying tumor mass. It was reported that not only can PDT (using the clinical photosensitizer Visudyne®) ablate spinal metastatic tumors,(*14*) but unexpectedly it also enhances vertebral mechanical stability.(*18, 19*) However, current photosensitizers are limited by their non-specific accumulation in normal tissues: e.g., Visudyne has non-specific uptake in the spinal cord limiting the therapeutic window which, in turn, reduces the aggressiveness of treatment in order to stay well within safe dose limits.(*14, 15*) Clearly, preservation of the spinal cord's structure and function is critical in the management of vertebral metastases. Photodynamic molecular beacons were introduced to provide an additional mechanism of selectivity in PDT over and above those due to photosensitizer and light targeting.(*20*) The beacons comprise a photosensitizer and a quencher moiety, linked, in the present case, by a MMP-cleavable peptide. They remain 'optically silent', i.e. photodynamically inactive, until transformed

into an activated state through cleavage of the linker, upon which both the PDT activity and PS fluorescence are restored, the latter providing the potential for real-time image guidance.(*20*) As beacons are only activated in the presence of these MMP metastases-specific proteases, normal tissues, including the spinal cord, should remain relatively protected.(*20*) Our vision is for beacon-PDT to result in complete destruction of intravertebral metastatic tumors without risk of spinal cord damage. This will have a potentially positive effect on bone integrity, increase the success and efficacy of vertebroplasty for spinal stabilization and eliminate local tumor recurrence. The intended impact of this novel intervention is the significant improvement in the quality of life for patients suffering from spinal metastases.

Body:

Zipper Photodynamic Molecular Beacons (ZMBs) (Appendix 1)(*21*)*:* During, our PDT beacon development, we co-opted a 'zipper' strategy to improve the PDT beacon's activation efficiency, specificity and intracellular delivery. As shown in Fig 2, such a 'zipper' beacon (ZMB) consists of four functional modules: 1) a protease cleavable peptide linker, 2) a polycation and a polyanion attached to each end of the linker which forms the 'zipper' structure via electrostatic attraction, 3) a PS conjugated to the polycation and 4) a quencher conjugated to the polyanion. The ZMB provides several advantages over classic beacons: 1) the formation of the 'zipper' through electrostatic attraction improves the silencing of the beacon by bringing PS and quencher into closer contact, 2) the polyanionic arm of the zipper prevents the probe from entering cells, by blocking the cell-penetrating function of the polycation, 3) the polycationic arm enhances cellular uptake of the PS after linker cleavage, and 4) quenching is no longer dependent upon the natural folding of the peptide linker, since the zipper is solely responsible for the inactive state (*21*). Together with a metastases-specific trigger, this novel ZMB mechanism provides a realistic opportunity to develop a PDT agent that will spare the spinal cord. A series of ZMB constructs with varying zipper arm lengths [zip(n)e, where n=the number of amino acids in both zipper arms]: zip3e, zip4e, zip5e, zip6e and zip8e were synthesized and tested.(*21*) In comparison to classic beacons, activation of zip8e resulted in a significantly higher fluorescence fold increase due to the enhanced quenching efficiency afforded by the zipper conformation (Fig 3). However, we observed a two-step activation process for this ZMB: 1) cleavage of the peptide linker and 2) dissociation of the zipper arms (Fig 3). This two-step activation creates a dilemma: on one hand, a stable zipper conformation is necessary to achieve maximum quenching efficiency; however, if the zipper structure is too stable, ZMBs are not fully activated due to the slow or inhibited the dissociation of the zipper arms. Based on the ZMB characteristics in Fig 3, 1) a stable zipper is formed when the zipper arm length is greater than 4 arginines and 4 glutamates (>zip4e), 2) the longer the zipper arm, the greater fluorescence quenching efficiency, and 3) the dissociation of the zipper arms in zip5e is a much more efficient process than that of zip8e. However, the practicality of 5-polyarginines assisting in the internalization of its cargo is questionable. Fig 4 demonstrates that 5-consecutive arginines cannot deliver cargo into cells, whereas 8 consecutive arginines show rapid uptake. Therefore, we determined the optimal ZMB requires an asymmetrical zipper conformation to balance between stable zipper formation, quenching efficiency, activation and intracellular delivery. However, although excellent activation kinetics was observed in solution with ZMB8r (zipper with eeeee and rrrrrrrr arms) when compared with classic PMB, the same improvement afforded by ZMB8r was not observed *in vitro*. Thus, further optimization of ZMBs is warranted. We hypothesize that the strength of the electrostatic attraction between zipper arms after linker cleavage are influenced by

biological environments. In order to optimize the ZMB design, not only should the stability of the zipper formation and the sensitivity of the zipper dissociation in response to linker cleavage be evaluated but favorable *in vitro* and *in vivo* activation and intracellular delivery must also be considered. Due to the closely related family of MMPs and their overlapping cleavage sequences, the peptide sequences used were recognized by more than one MMP. However, the most suitable MMP cleavage sequence was determined to be GPL*G*L*ARK as this sequence is cleaved specifically by the family of MMP (Fig 5). Furthermore, for the spinal metastases application, this is not disadvantageous as the family of MMP has been implicated to play a role in bone development and bone matrix solubilization. Since tumor cells have already hi-jacked the normal osteolytic cycle, MMP activation further amplify ZMB activation furthering the disruption of the vicious tumor-bone cycle.

Preclinical studies to evaluate the specific PDT beacon activation in spinal metastases (Appendix 1) *(22):* For proof-of-concept, we demonstrated the metastasis-selective mechanism of PDT beacons using an established *in vivo* model: luciferase and GFP transfected human breast cancer cells (MT-1) metastasize to the vertebral column 1-2 weeks following intracardiac injection into 4-5 week old female athymic rats (Hsd:RH-*Foxn1*^{rnu}) (*14-19, 23*). Bioluminescence imaging using a Xenogen IVIS imaging system has been shown by us (*14, 15, 17-19*) and others (*24, 25*) as a powerful and quantitative tool to monitor bone metastases in small animals. The MMP-specific beacon activation was assessed by ex vivo fluorescence imaging at 2, 4, 12 and 24 h after a 3mg/kg intravenous injection of the beacons. For this, the animals were euthanized at the above mentioned time points and the spines excised and sagitally cut. Using a CRI multispectral Maestro *InVivo* imaging System and a Zeiss LSM510 META laser scanning confocal microscope (excitation: 633nm, emission: > 650nm), beacon activation by fluorescence detection was overlaid with the GFP signal of MT-1 cells, indicating the specific activation of the beacons *in vivo* by spinal metastases (Fig 6 and 7, Appendix 2) (*22*). Regardless of the imaging time point, no beacon activation was observed within the spinal cord. These results clearly demonstrate that 1) activation of PDT beacon is mediated by spinal metastases-expressing MMPs, 2) activated beacons can reach and target the intravertebral tumors and 3) these beacons are inactive within the spinal cord, indicating the ability of beacons to preserve the spinal cord, a critical tissue, during PDT treatment (*22*).

Preclinical studies evaluating PDT beacon' efficacy for treating spinal metastases: At 2 or 4 h post-injection (the highest beacon activation signal at tumor sites), an optical fiber was placed adjacent to the outer cortical layer of the target spinal body using X-ray guidance. A light dose of 150J in the lumbar spine resulted in tumor regression without normal tissue damage. Histological analysis of treated vertebrae indicated PDT-induced destruction of MT-1 metastases (Fig 8). These preliminary results demonstrate PDT beacon's ability to specifically destroy spinal metastases in our animal model (Fig 9).

Key Research Outcomes:

- Determined the most suitable MMP cleavage sequence for improved specificity towards breast cancer vertebral metastases
- Narrowed down the optimized ZMB construct to three potential zipper arm candidates Zip6e, Zip7e, or Zip8e
- Demonstrated the specification activation of MMP PDT beacons is mediated by spinal metastases-expressing MMPs

- Demonstrated that only activated MMP PDT beacons can target intravertebral tumors
- Demonstrated that activated MMP PDT beacons are inactive within the spinal cord indicating the ability of beacons to preserve the spinal cord, a critical tissue, during PDT treatment.
- Demonstrated preliminarily the PDT beacon's ability to specifically destroy spinal metastases *in vivo*

Reportable Outcomes:

- Manuscript: Liu, T.W., Akens, M.K., Chen, J, Wise-Milestone, L., Wilson, B.C., Zheng, G. *Photodynamic Molecular Beacons in Breast Cancer Vertebral Metastases: Imaging Validation of Beacon Specificity*. Clinical Cancer Research, under review, 2011.
- Manuscript: Chen, J., Liu, T.W., Lo, P.C., Wilson, C.B., Zheng, G. *"Zipper" Molecular Beacons: A Generalized Strategy to Optimize the Performance of Activatable Protease Probes.* Bioconjug Chem, Sept. 2009
- Abstract: Liu, T.W., Akens, M.K., Chen, J, Wise-Milestone, L., Wilson, B.C., Zheng, G, "Specific activation of photodynamic molecular beacons: an image-guided therapeutic approach for vertebral metastases." Oral presentation, European Conferences on Biomedical Optics, May 2011, Munich, Germany.
- Abstract: Liu, T.W., Akens, M.K., Chen, J, Wise-Milestone, L., Wilson, B.C., Zheng, G, "Specific Activation of Photodynamic Molecular Beacons: An Image -Guided Therapeutic Approach for Vertebral Metastases." Poster presentation, 5th International Graduate Summer School Biophotonics '11, May 2011,Backafallsbyn, Ven in Sweden.
- Abstract: Liu, T.W., Akens, M.K., Chen, J, Wise-Milestone, L., Wilson, B.C., Zheng, G, "Photodynamic Molecular Beacons: Image-Guided Therapeutic Approach for Vertebral Metastases." Oral presentation, Optics Within Life Sciences, September 2010 Quebec City , Canada.
- Abstract: Liu, T.W., Akens, M.K., Chen, J, Wise-Milestone, L., Wilson, B.C., Zheng, G, "Molecular Beacon-Guided Surgical Resection of Primary Spinal Neoplasms." Poster presentation, September 2010 , UK.
- Abstract: Liu, T.W., Akens, M.K., Chen, J, Wise-Milestone, L., Wilson, B.C., Zheng, G, "Photodynamic Molecular Beacons: Image-Guided Therapeutic Approach for Vertebral Metastases." Poster presentation award winner Gordon conference: Lasers in Medicine and Biology, July 2010**,** New Hampshire, USA.
- Abstract: Liu, T.W., Chen, J, Wilson, B.C., Zheng, G, "Zipper Molecular Beacons: a generalized methodology for activatable photodynamic molecular beacons." Poster presentation, Ontario Cancer Institute of Research Annual Symposium Meeting, Feb 2010, Nottawasaga, Canada.

Conclusion:

Photodynamic molecular beacons may be a key component in the use of PDT as a new, minimally-invasive, safe and effective therapy for the management of patients with spinal metastases when used, for example, as an adjuvant to minimally-invasive surgical techniques such as vertebroplasty or kyphoplasty for mechanical stabilization.(*14, 16, 17*) We have recently started a Phase I clinical trial with the clinically-approved photosensitzer Visudyne (QLT Inc,

Vancouver, BC, Canada), in which the objective is to debulk the intravertebral space-occupying tumor mass that often impedes these surgical approaches. However, based on preclinical studies(*14*, *15*), the therapeutic window is likely to be limited by the non-specific uptake of the photosensitizer by healthy tissues, including the spinal cord, which will restrict the drug and light doses that can be used safely. MMP PDT beacons potentially address this limitation. We have demonstrated the specific activation of MMP PDT beacons by MMP-expressing vertebral metastases in a relevant preclinical model illustrating defined kinetics and the ability to target intravertebral metastatic tumors with minimal uptake or activation in the spinal cord. This is a first step in the further development of such beacons and their potential translation into useful clinical tools for a range of applications. To this end, as mentioned above, we are currently evaluating the therapeutic window of MMP PDT beacons PDT, the effect of MMP PDT beacons PDT-induced tumor destruction within the vertebrae and optimizing the ZMB design. As we are in the final stages of ZMB optimization, *in vitro* studies validating the specific activation with favorable kinetics and intracellular delivery by metastatic human breast cancer cells will soon be underway. Our vision is for ZMB-PDT to result in complete destruction of intravertebral metastatic tumors without risk of spinal cord damage. This will have a potentially positive effect on bone integrity, increase the success and efficacy of vertebroplasty for spinal stabilization and eliminate local tumor recurrence. The intended impact of this novel intervention is the significant improvement in the quality of life for patients suffering from spinal metastases.

References:

1. V. A. Siclari, T. A. Guise, J. M. Chirgwin, *Cancer metastasis reviews* **25**, 621 (Dec, 2006).
2. L. A. Kingsley, P. G. Fournier, J. M. Chirgwin, T. A. Guise, *Mol Cancer Ther* **6**, 2609 (Oct, 2007).
3. G. R. Mundy, *Nature reviews* **2**, 584 (Aug, 2002).
4. C. E. Brinckerhoff, L. M. Matrisian, *Nat Rev Mol Cell Biol* **3**, 207 (Mar, 2002).
5. K. Kessenbrock, V. Plaks, Z. Werb, *Cell* **141**, 52 (Apr 2).
6. J. K. Woodward, I. Holen, R. E. Coleman, D. J. Buttle, *Bone* **41**, 912 (Dec, 2007).
7. T. A. Guise, *Genes Dev* **23**, 2117 (Sep 15, 2009).
8. I. American Cancer Society. Breast Cancer Facts & Figures 2009-2010. Atlanta: American Cancer Society.
9. M. A. Finn, F. D. Vrionis, M. H. Schmidt, *Cancer Control* **14**, 405 (Oct, 2007).
10. R. H. Bartels, Y. M. van der Linden, W. T. van der Graaf, *CA: a cancer journal for clinicians* **58**, 245 (Jul-Aug, 2008).
11. B. C. Wilson, M. S. Patterson, *Physics in medicine and biology* **53**, R61 (May 7, 2008).
12. J. P. Celli *et al.*, *Chem Rev* **110**, 2795 (May 12, 2010).
13. S. Pervaiz, M. Olivo, *Clin Exp Pharmacol Physiol* **33**, 551 (May-Jun, 2006).
14. M. K. Akens *et al.*, *Breast cancer research and treatment* **119**, 325 (Jan, 2010).
15. M. K. Akens *et al.*, *Photochemistry and photobiology* **83**, 1034 (Sep-Oct, 2007).
16. S. Burch *et al.*, *J Orthop Res* **23**, 995 (Sep, 2005).
17. S. Burch *et al.*, *Journal of biomedical optics* **10**, 034011 (May-Jun, 2005).
18. E. Won *et al.*, *Spine* **35**, 272 (Feb 1, 2010).
19. E. Won *et al.*, *Breast cancer research and treatment*, (Jan 12, 2010).
20. G. Zheng *et al.*, *Proceedings of the National Academy of Sciences of the United States of America* **104**, 8989 (May 22, 2007).
21. J. Chen, T. W. Liu, P. C. Lo, B. C. Wilson, G. Zheng, *Bioconjugate chemistry*, (Sep 14, 2009).
22. T. W. Liu *et al.*, *Clinical Cancer Research, under review*, (2011).
23. S. Burch, S. K. Bisland, B. C. Wilson, C. Whyne, A. J. Yee, *Clinical orthopaedics and related research* **454**, 230 (Jan, 2007).
24. C. P. Klerk *et al.*, *Biotechniques* **43**, 7 (Jul, 2007).
25. A. Sato, B. Klaunberg, R. Tolwani, *Comp Med* **54**, 631 (Dec, 2004).

Appendices:

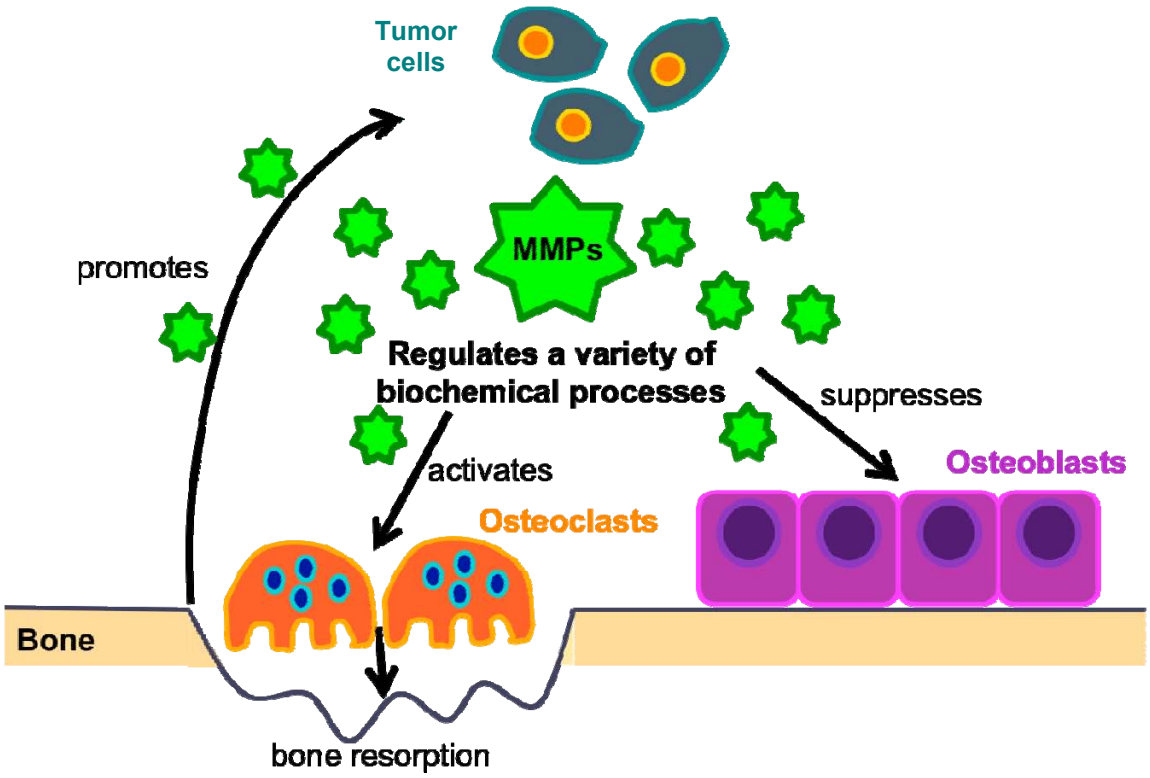

Figure 1. The involvement of MMPs in the vicious tumor-bone spinal metastases cycle. MMPs play central roles in helping the tumor cells to destroy the delicate balance between bone formation (osteoblasts) and degradation (osteoclasts) that maintains the bone integrity. By targeting MMPs, we may not only destroy spinal metastases but also disrupt the vicious tumour-bone cycle within the vertebral body.

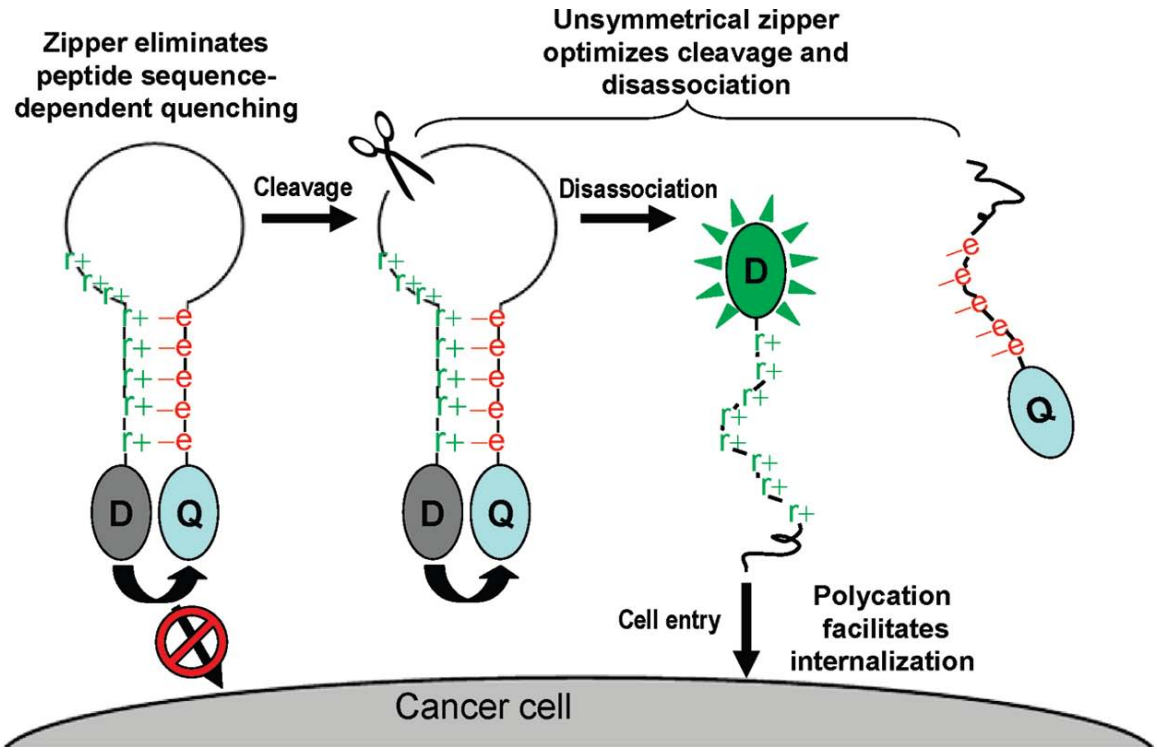

Figure 2. Zipper molecular beacon (ZMB) design: the "zipper" is composed of a pair of polycation and polyanion arms holding the photosensitizer (PS) and quencher (Q) in close proximity due to electrostatic attraction. This results in silenced PS activity independent of peptide linker variations. Upon specific enzymatic cleavage of the linker, the PS and Q dissociate, resulting in PS photoactivity and unleashing the polycation, which increases cellular uptake.

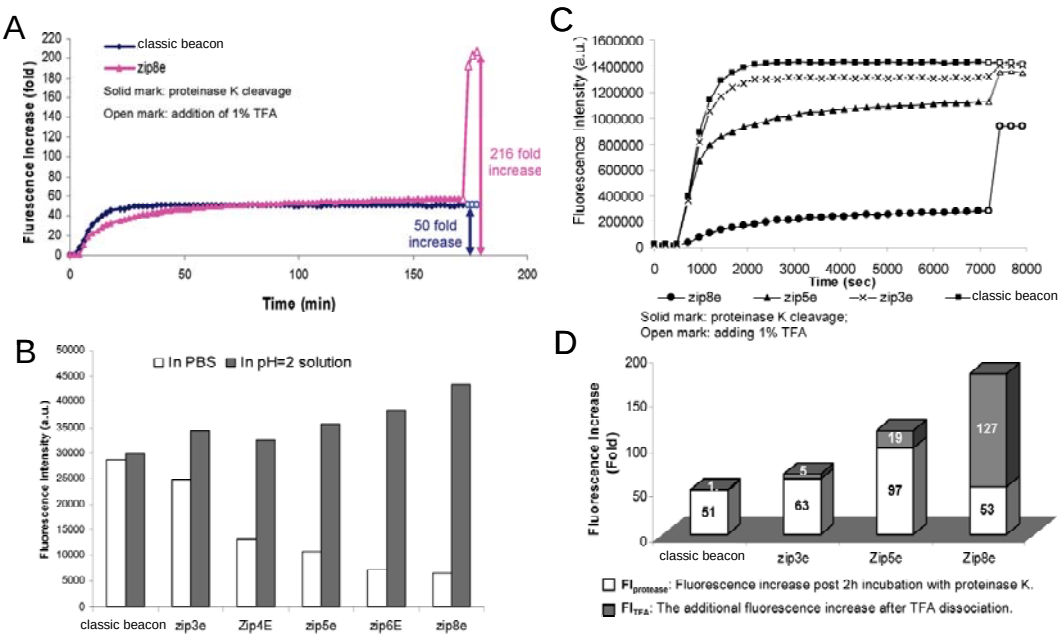

Figure 3. Evaluation of ZMB constructs. A) Comparison of the protease-mediated activation of ZMB and classic beacons. Cleavage kinetic profiles of probes depict increase in fluorescence after 3 h protease incubation and post TFA-induced disassociation.. B) Fluorescence emission and zipper stabilityof intact ZMBs in PBS and low pH condition (pH) 2). C) Protease cleavage monitored by real time fluorescence. D) Evaluation of the two-step activation of ZMB: Fluorescence release after protease cleavage of ZMB linker ($FI_{protease}$) and fluorescence release after zipper dissociation due to low pH (FI_{TFA}) values for ZMBs and classic beacons.

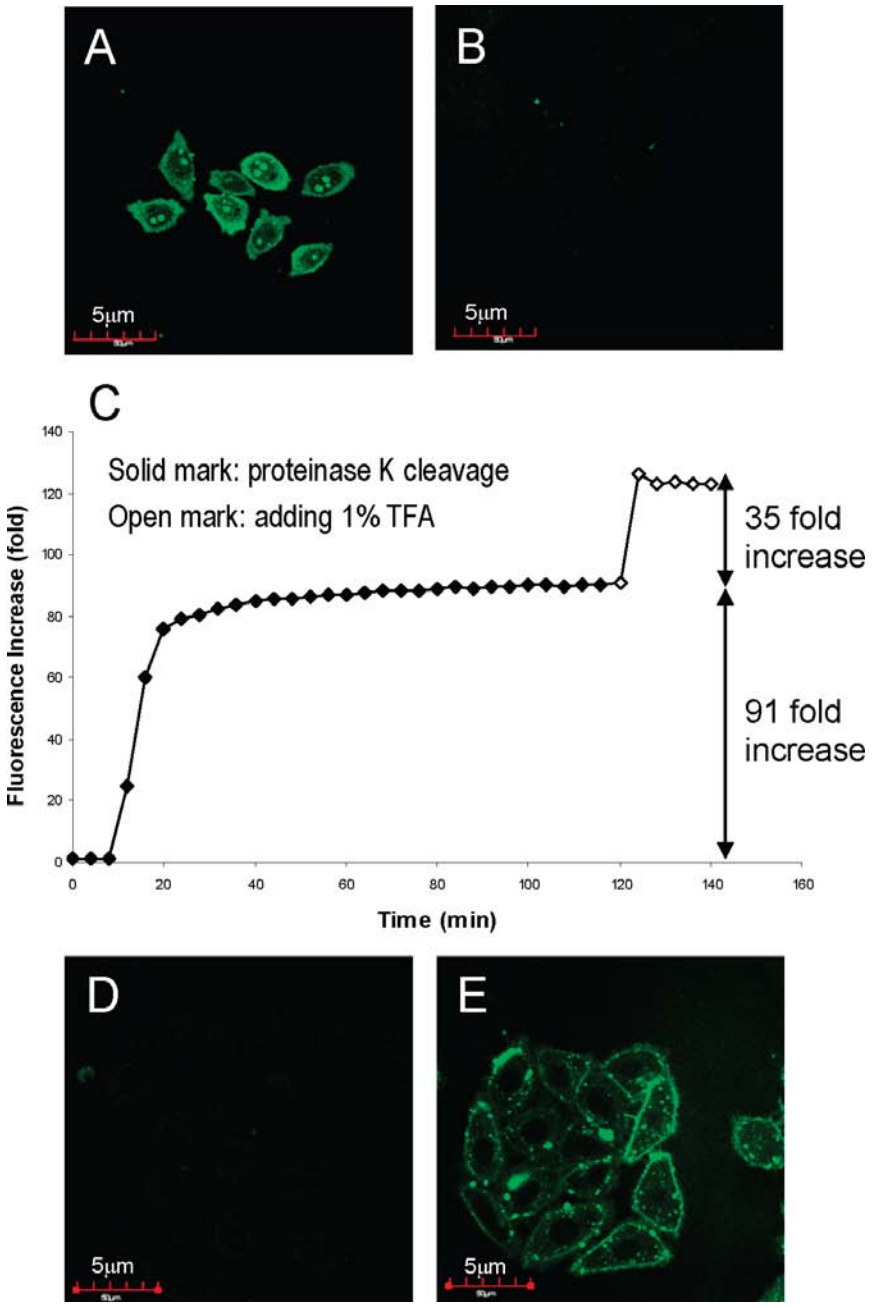

Figure 4. Confocal images of 5 μM (A) Fmoc-D(rrrrrrrr)-K(FITC) and (B) Fmoc-D(rrrrr)-K(FITC) in MT1 cells showing fluorescence in each case.(C) Activation kinetics of zip5e8r by Proteinase K in PBS. Confocal images of cell uptake of (D) nonzip1 and (E) zip5e8r at 30 min after cleavage by 3-day-old MT1 cell culture media.

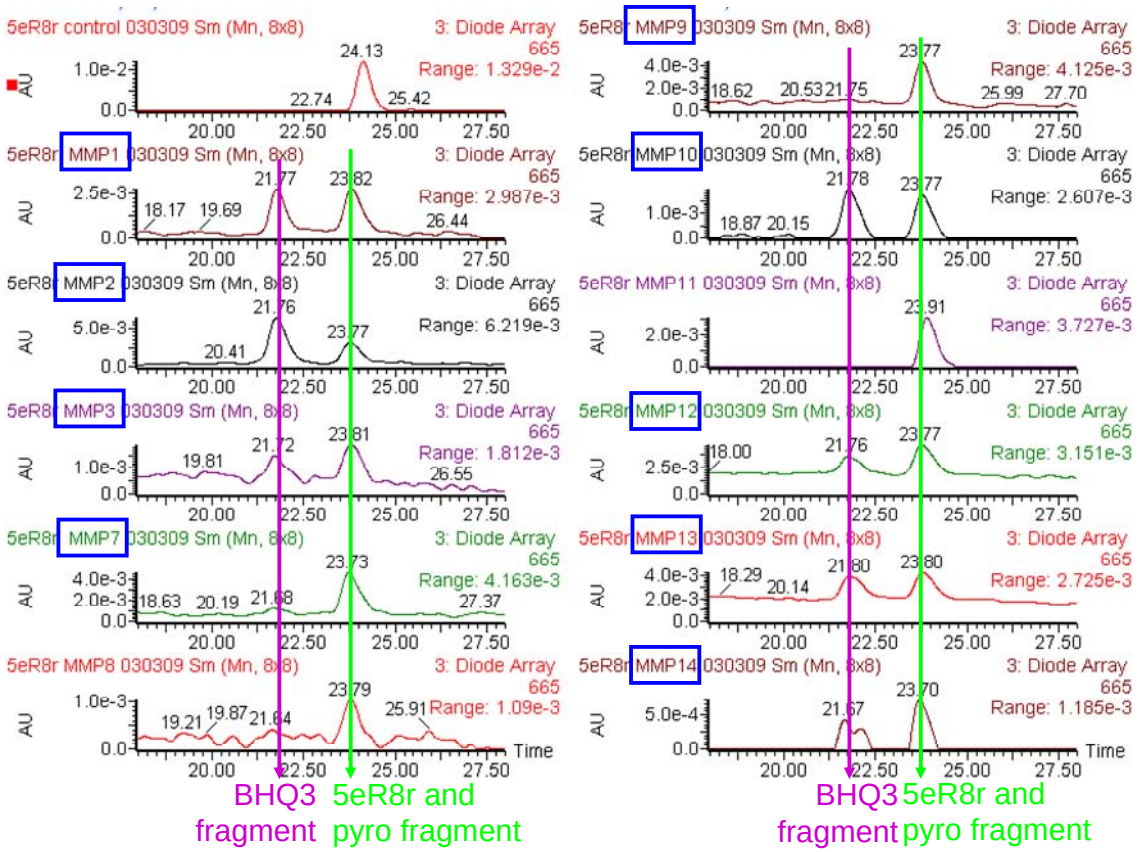

Figure 5. HPLC chromatograms demonstrating the specific cleavage of ZMB8r by MMPs. *Unpublished data*

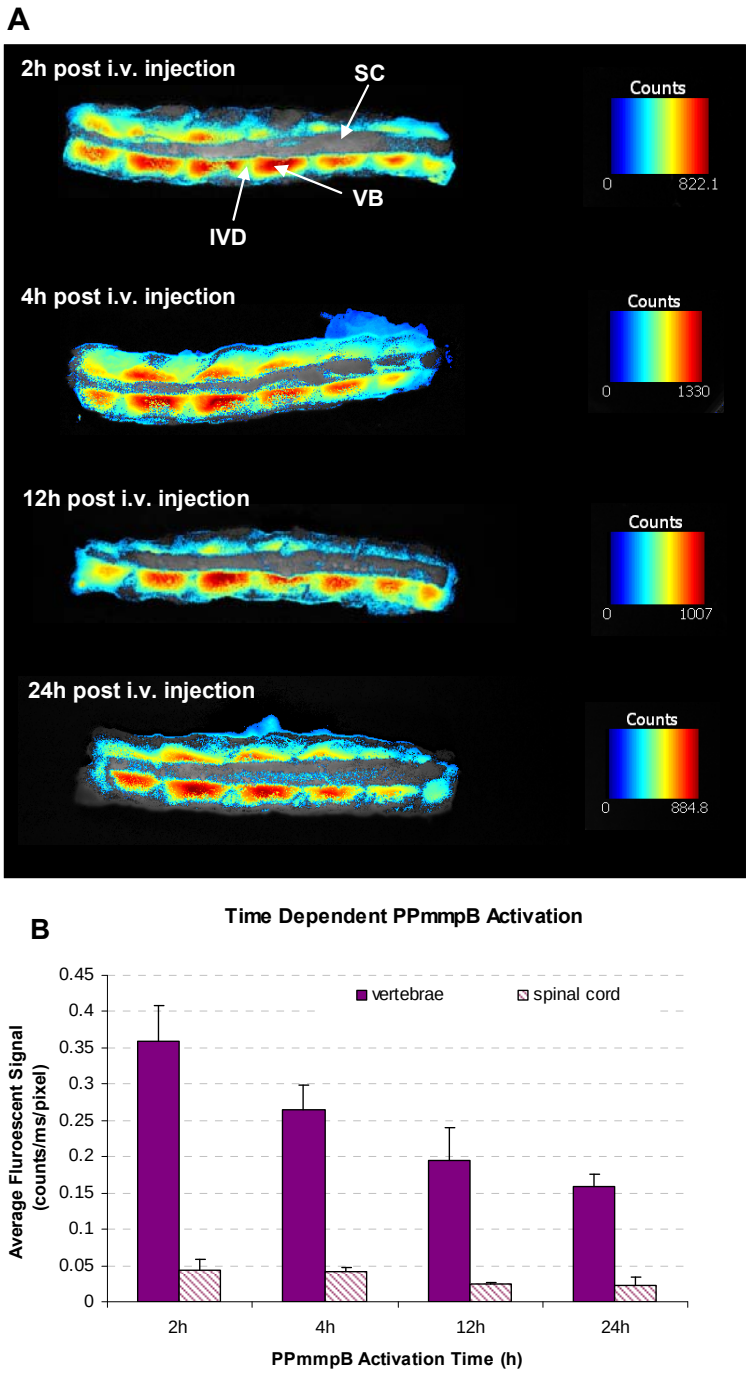

Figure 6. Time-dependent activation of beacons by vertebral metastases imaged *ex vivo*. A) Composite fluorescence images at 2, 4, 12 and 24h after intravenous injection of 3 mg/kg of beacons: SC – spinal cord, VB – vertebral body, IVD – intervertebral disc. B) Average fluorescent signal comparing the vertebrae and spinal cord: * indicates statically significant difference between 2h versus 12h and 24h time points of beacon activation in the vertebrae (n=4 for 2 and 4h time points, n=2 for 12 and 24h). Note: there is no beacon activation within the spinal cord. *Unpublished data (under review)*

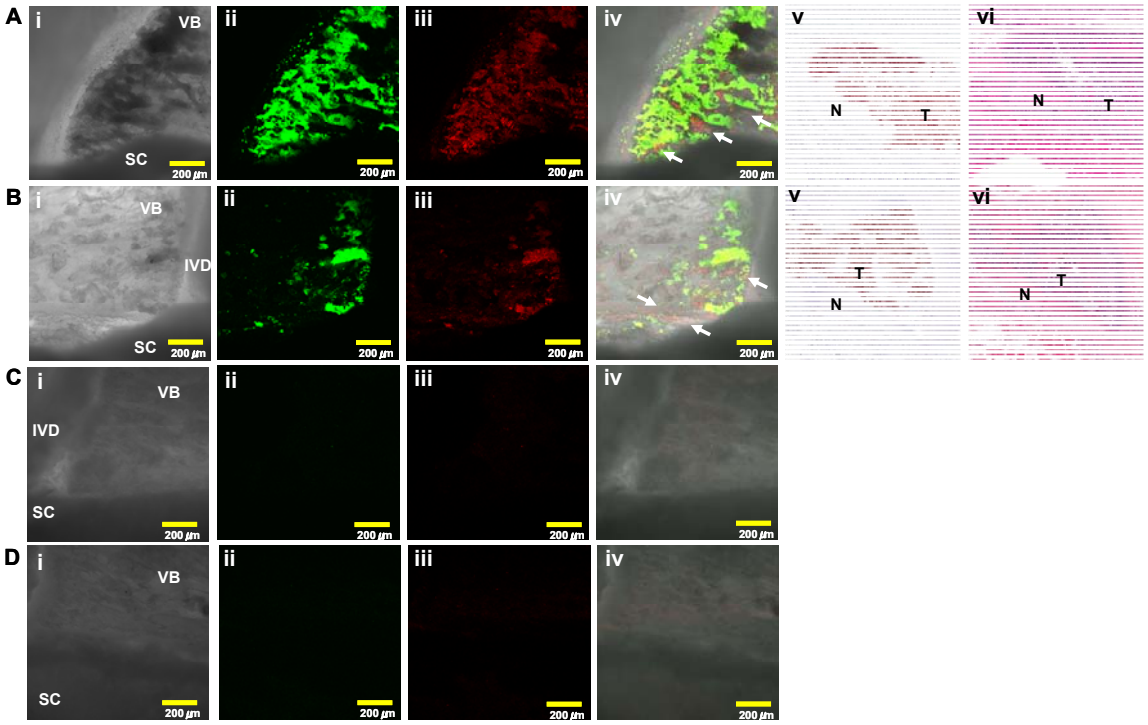

Figure 7. Micrographs of vertebrae at 2h post i.v. injection of 3mg/kg beacons into (A, B) MT-1 tumor-bearing rats, (C, D) healthy rats. i) brightfield image, ii) GFP image showing the MT-1 cells, iii) activated beacon, iv) merged images of GFP and activated beacon: VB – vertebral body, IVD – intervertebral disc, SC – spinal cord. v) hEGFr and vi) H&E stained sections (T – tumor, N – normal). *Unpublished data (under review)*

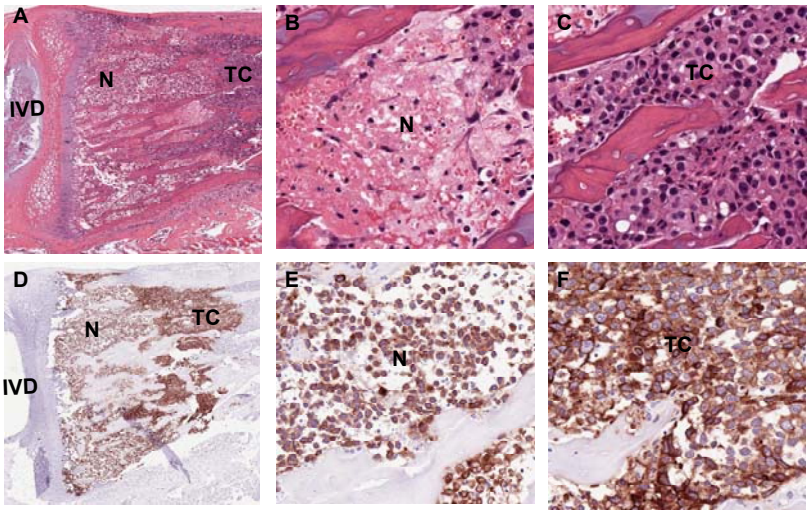

Figure 8. Histological slides of H&E (A, B, C) and hEGFr immunohisto staining (D, E, F) of PDT treated (3mg/kg beacon; 150J) vertebrae. *TC* intact tumour cells, *N* apoptotic and necrotic tumour cells (non-viable tumour areas after PDT) and *IVD* intervertebral disc. *Unpublished data*

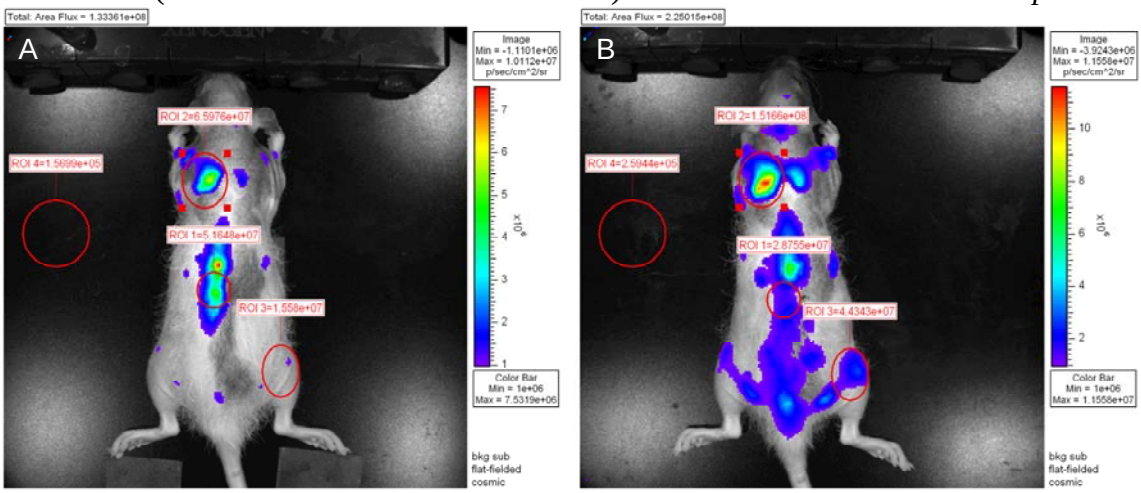

C

Area	Bioluminescent signal (Post PDT(B) /Pre PDT (A))
PDT site (ROI 1)	0.55
Shoulder (ROI 2)	2.30
Femur (ROI 3)	2.86

Figure 9. Bioluminescence images 14 days after tumour cell injection. A) Prior to PDT treatment and B) 24 h post PDT (3 mg/kg; 150 J). ROI 1: PDT treated area, ROI 2: shoulder, ROI 3: femur tumour, ROI 4: background signal. C) Tumour growth based on ratio of bioluminescent signals before and after light treatment. ROI 4 (background signal) was subtracted from measurements. Values <1 indicate a decrease in tumour size, values >1 indicate an increase in tumour size. *Unpublished data*

COMMUNICATIONS

"Zipper" Molecular Beacons: A Generalized Strategy to Optimize the Performance of Activatable Protease Probes

Juan Chen, Tracy W. B. Liu,† Pui-Chi Lo, Brian C. Wilson, and Gang Zheng*

Department of Medical Biophysics, Ontario Cancer Institute, University of Toronto, Toronto, Ontario M5G 1L7, Canada.
Received May 7, 2009; Revised Manuscript Received August 31, 2009

We report the proof-of-principle concept for zipper molecular beacons (ZMB) comprising an asymmetrical polyarginine/polyglutamate electrostatic "zipper" hairpin-linked fluorophore−quencher pair. The objective is to balance maximal quenching efficiency and optimal two-step activation (protease cleavage/zipper dissociation), while enhancing target cell uptake. This strategy also eliminates the peptide sequence dependence of conventional protease beacons. This ZMB concept is a generalizable approach to improve the functionality of a wide range of diagnostic/therapeutic probes through a simple switching of substrate sequences.

INTRODUCTION

Optical molecular imaging has become a powerful tool for biochemical and cellular studies (*1*). With the continual development of peptide-based "smart probes", the *in vivo* optical imaging of specific molecular targets, biological pathways, and disease progression is gaining momentum. Many of the initial fluorescent probes had limited image contrast due to poor target specificity. Hence, activatable optical probes (*2*−*9*) that require enzyme-triggered separation of an inhibitory moiety from an active partner were developed. More recently, we and others have extended this concept to photodynamic molecular beacons (*10*−*14*) for increased specificity in photodynamic therapy. These activatable protease probes comprise an enzyme-specific linker with a fluorophore (or photosensitizer) and quencher conjugated at its opposite ends. The probes are inactive until the linker is cleaved by a target-specific enzyme. Although such activatable imaging and therapeutic beacons have shown great promise, several challenges have arisen.

First, the quenching depends on the natural peptide folding of the enzyme-specific linker. Thus, the probes are limited to sequences with natural conformations that bring the quencher and active moiety in close proximity in order for effective silencing to occur. In other words, different peptide sequences have different background fluorescence. A second concern is most protease-specific probes are activated extracellularly, so that the activated probes may diffuse to nontarget cells/tissues before target cell uptake occurs. Third, probes that target soluble proteases may be activated at sites distant from the target due to leakage of the enzyme from the target cells into the general circulation (*15*−*17*), thereby contributing to background signal and reduced contrast. Lastly, the probes use nonspecific/passive delivery to the target cells/tissues, which is suboptimal.

Recently, the concept of activatable cell-penetrating peptides (ACPP) was introduced to address the passive delivery of first-generation activatable optical probes. These are based on the electrostatic formation of a polycation/polyanion "zipper", whose linker can be selectively cleaved by a protease to locally unleash the delivery function of cell-penetrating peptides (CPP) (*15*−*17*). The underlying mechanism is functionally reminiscent of molecular beacons themselves that require enzyme-triggered separation of an inhibitory moiety from an active partner: here, the separation is between a polyanionic peptide (polyanion) and a polycationic peptide (polycation). Inclusion of a quencher may improve imaging contrast by suppressing the active partner before cleavage of the linker (*15*). The concept is illustrated in Scheme 1.

MATERIALS AND METHODS

All amino acid derivatives and the Sieber amide resin were purchased from Novabiochem (San Diego, CA, USA). The black hole quencher3 carboxylic acid succinimdyl ester (BHQ3-NHS) was obtained from Biosearch Technologies (Novato CA, USA). The pyropheophorbide carboxylic acid succinimidyl ester (Pyro-NHS) was prepared according to a published procedure (*18*). Other chemicals were obtained from Aldrich (Oakville, ON) and were used as received. Reverse-phase HPLC was preformed on a XBridgeTM-C8 column (2.5 μm, 4.6 × 150 mm) using a Waters 2695 controller with a 2996 photodiode array detector and a Waters ZQTM mass detector (Waters Limited, Mississauga, ON).

Synthesis of ZMB. The peptide sequence Fmoc-[D-Glu(Ot-Bu)]$_x$-protected activatable peptide linker-[D-Arg(Pbf)]$_y$Lys(Mtt) was synthesized on the Sieber resin according to a solid-phase peptide synthesis (SPPS) protocol using a PS3 peptide synthesizer (Protein Technologies) with commercially available *N*-α-Fmoc-protected amino acids. After the last Fmoc group had been removed from the peptide resin with 20% piperidine in *N*,*N*-dimethylformamide (DMF), the resin was washed with DMF. BHQ3-NHS was then coupled to the N-terminal of the peptide in DMF with *N*,*N*-diisopropylethylamine (DIPEA) (BHQ3/peptide = 3:1 molar ratio). The mixtures were shaken under argon overnight at room temperature. The acquired dark-blue resin was washed with DMF and then treated with 95%

* Correspondence to G. Zheng, TMDT 5-363, 101 College St, Toronto, ON M5G 1L7, Canada. Fax: 416-581-7666, gang.zheng@uhnres.utoronto.ca.
† First two authors contributed equally to this work.

10.1021/bc900207k CCC: $40.75
Published on Web 09/14/2009

Scheme 1. Universal Zipper Molecular Beacon Design[a]

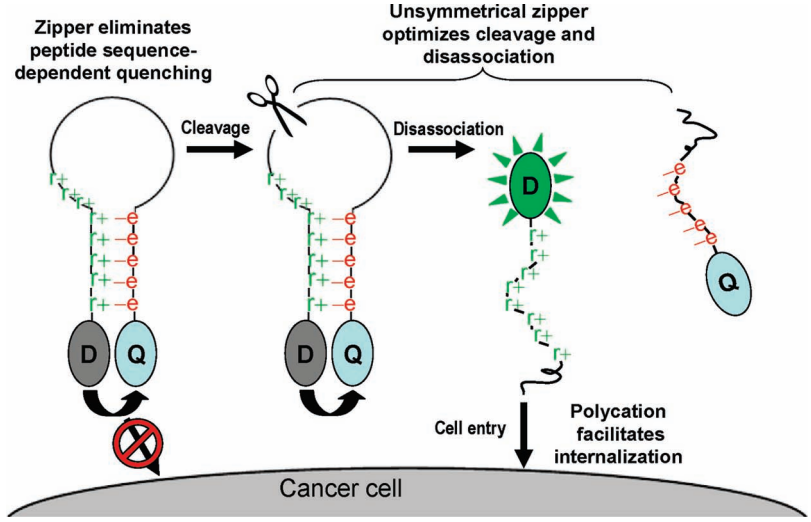

[a] The "zipper" is composed of a pair of polycation and polyanion arms holding the dye (D) and quencher (Q) in close proximity due to electrostatic attraction. This results in silenced dye activity independent of peptide linker variations. Upon specific enzymatic cleavage of the linker, the dye and quencher dissociate, resulting in dye photoactivity and unleashing the polycation, which increases cellular uptake.

trifluoroacetic acid (TFA) with 5% triisopropylsilane (Tis) to remove the protected groups on the peptide and cleave the peptide from the resin. After removing the solid support by filtration, the filtrates were concentrated and precipitated by diethyl ether to give the BHQ3-conjugated peptide, BHQ3-$_D$(e)x-activatable peptide linker-$_D$(r)yK(NH_2). The peptide was then reacted with Pyro-NHS in anhydrous DMSO with 1% DIPEA at ambient temperature for 6 h. The reaction mixture were then purified by HPLC to give pure BHQ3-$_D$(e)x-activatable peptide linker (r)yK(Pyro), which were characterized using UV−vis and ESI mass spectroscopy.

Synthesis of Controls. The synthesis of nonquencher control, Pyro-GPLGLARK (PP), and nonzipper control, Pyro-GPLGLARK-(BHQ3) (nonzip1), were reported previously (*12*). Nonzip2, Pyro-RPLALWRSK(BHQ3), was synthesized using the similar procedure as nonzip1. FITC-labeled polycation control, Fmoc-$_D$(r)x-K(FITC), was synthesized as follows: Fmoc-[D-Arg-(Pbf)]x-K(Mtt) was synthesized on the Sieber resin. The resin was then treated with 95% TFA with 5% Tis to remove the protected groups on the sequence and cleave the sequence from the resin. The acquired Fmoc-$_D$(r)x-K(ε-NH_2) was then reacted with fluorescein isothiocyanate (FITC) in anhydrous DMSO with 1% DIPEA at ambient temperature for 6 h. The reaction mixture were then purified by HPLC to give pure Fmoc-$_D$(r)x-K(FITC). Nonquencher ACPP control, Fmoc-$_D$(e)$_5$GPLGLA$_D$(r)$_8$K(Pyro) (Pyro-ACPP), was synthesized using a similar protocol to Fmoc-$_D$(r)x-K(FITC). The differences are in (1) replacing the peptide sequence and (2) conjugating Pyro-NHS on the C-terminal rather than FITC.

pH Dissociation Assay of ZMB. 0.5 μM of ZMB samples were prepared in adjusted PBS solutions with different pH (pH = 2, 3, 4, 5, 6, 7, 8, 9, 10, 11, 13). Their fluorescence emission was measured on a HORIBA FluoroMax-4 spectrofluorometer (excitation 650 nm, emission 675 ± 5 nm). Using the sample of pH = 7 as reference, the fluorescence increase in different pH conditions was calculated to evaluate the structure stability of ZMB.

Activation Studies. ZMB or nonzipper probes (1 nmol) were first dissolved in 2.5 μL of DMSO and 0.5 μL of Tween 80. The solution was diluted with 1 mL of phosphate-buffered saline (PBS) or minimum essential medium (MEM) Eagle cell media, and then incubated with 10 μL of human Proteinase K (2 μg) (ZMB/Proteinase K ∼ 50:1 molar ratio). The activation was monitored by the fluorescence increase, which was calculated by normalizing the sample's fluorescence emission on real-time to its initial fluorescence. $FI_{protease}$ and FI_{TFA} were used to define the fluorescence increase at 2 h post-Proteinase K cleavage and following fluorescence increase after adding 1% TFA to the cleavage solution.

Evaluation of Polycation Delivery Capability. MT1 cells were grown to 60% confluence in Nunc Lab-TekII-CC2 chambered slides. Eagle's minimum essential medium (MEM) medium with 10% fetal bovine serum containing 5 μM of Fmoc-$_D$(rrrrr)-K(FITC) and Fmoc-$_D$(rrrrrrrr)-K(FITC) were added and incubated for 10 min at 37 °C. The cells were washed 3 times with PBS. The chamber slides were then imaged on an Olympus FluoView 1000 laser scanning confocal microscope equipped with a 488 nm argon laser.

Evaluation of Cell Uptake of ZMB before and after Activation. (1) Preparing nonactivation sample: Fresh MEM medium with 10% fetal bovine serum (without proteases) was used to prepare a 10 μM concentration of the probes. (2) Preparing postactivation samples: MT1 cells were grown in Nunc Lab-TekII-CC2 chambered slides for 3 days. A 10 μM concentration of the probes were prepared in this 3-day-old cell incubation medium (contains secreted proteases including MMP7) and incubated until the peptide linkers of probes were cleaved (monitored by HPLC). (3) Confocal study: 200 μL of these samples were incubated with MT1 cells in the chamber slides for 30 min. The chamber slides were washed with PBS 3 times and then imaged by a confocal microscope equipped with a 633 nm He−Ne laser.

RESULTS AND DISCUSSION

To test this concept, we designed a ZMB with four functional modules: (1) a protease cleavable peptide as the linker, (2) a polycation and a polyanion attached to each end of the linker, forming a "zipper" structure via electrostatic attraction, (3) pyropheophorbide as a fluorescent dye (D), and (4) a Black Hole Quencher 3 as a quencher (Q), conjugated to the end of the polycation and polyanion, respectively. As shown in Scheme 1, the zipper provides several potential advantages: (1) the formation of the polycation/polyanion "zipper" through electrostatic attraction improves the silencing of the beacon by bringing D and Q into closer contact, (2) a "hairpin" conformation of the substrate sequence occurs as a result of the zipper,

Table 1. Abbreviations of Protease Probes

probe	sequence
nonzip1	Pyro-GPLGLARK(BHQ3)
nonzip2	Pyro-RPLALWRSK(BHQ3)
zipXe	BHQ3-$_D$(e)$_X$GPLGLA$_D$(r)$_X$K(Pyro)
zip8e2	BHQ3-$_D$(e)$_8$ RPLALWRS$_D$(r)$_8$K(Pyro)
zip5e8r	BHQ3-$_D$(e)$_5$ GPLGLA$_D$(r)$_8$K(Pyro)
PP	Pyro-GPLGLARK

improving the cleavage rate of the enzyme-specific linker, (3) the polyanionic arm of the zipper prevents the probe from entering cells, by blocking the cell-penetrating function of the polycation, (4) the polycationic arm enhances cellular uptake of the dye after linker cleavage, and (5) quenching is no longer dependent upon the natural folding of the peptide linker, since the zipper is solely responsible for the "dormant" state. In the presence of a target protease, the peptide linker is first specifically cleaved; the Q-attached polyanion then dissociates from the D-attached polycation, becoming photoactive, and unleashes the polycation, which enhances the delivery of the activated dye locally into the target cells.

In order to examine the effect of the zipper conformation on the photophysical properties, two matrix metalloproteinase 7 (MMP7)-specific peptide sequences, GPLGLARK (*19*) and RPLALWRSK (*20*), were used to synthesize two ZMBs, zip8e and zip8e2, and their corresponding nonzipper controls, nonzip1 and nonzip2 (see Table 1). Eight consecutive D-arginines, $_D$(rrrrrrrr), and D-glutamates, $_D$(eeeeeeee), were selected as the polycation and polyanion, respectively, as these can assemble into a stable zipper hairpin structure (*15*). D-Amino acids were used for the zipper arms, since they are stable against proteolysis (*21*). Also, D-amino acid-based polycationic peptides present similar cell penetrating capabilities to the natural L-amino acids (*22*).

The fluorescence emission of these probes was evaluated, normalized to that of the nonquencher probe, PP. As shown in Figure 1C, a marked difference in the fluorescence of nonzip1 and nonzip2 was observed (<2% and 27.2%, respectively). There was only a slight difference in the length and solubility of the peptide linkers in nonzip1 and nonzip2, indicating that the fluorescence quenching efficiency in the nonzipper probes does depend on the natural folding of the linkers (Supporting Information Figure S1 and Table S1, HPLC retention time). However, with the inclusion of the zipper, the quenching efficiencies were enhanced, with the fluorescence of zip8e and zip8e2 being reduced to 0.4% and 0.9%, respectively. This comparable quenching in zip8e and zip8e2 indicates that the quenching dependence on the natural folding of the peptide linker has been eliminated. Moreover, in aqueous solution, the specific absorption peaks of Pyro (414 nm) and BHQ3 (676 nm) in zip8e were shifted relative to their corresponding nonzipper probes (nonzip1) (Figure 1A). By adjusting the solution to a low pH condition (pH = 2) to neutralize the polyanion sequence and unfold the peptide sequence, the fluorescence of zip8e was increased 4-fold and its specific absorption was restored (Figure 1B), while nonzip1 did not show any obvious changes. Therefore, the enhanced quenching efficiency in the ZMB is presumably the result of both the improved fluorescence resonance energy transfer (FRET) effect and the ground-state complex quenching (contact quenching) caused by annealing D and Q through the electrostatic attraction of the zipper arms.

We next verified the electrostatic nature of the zipper conformation using a pH dissociation assay. As shown in Figure 1D, the fluorescence values of both zip8e and nonzip1 were very stable at pH $\sim$ 5−9. At pH < 5, the fluorescence of zip8e increased continually with decreasing pH, while that of nonzip1 was unchanged. This suggests that the zipper conformation disassociates at pH around 4, coinciding with the isoelectric point of the glutamic acid, and so confirming the electrostatic nature of the zipper conformation. The fluorescence increase at pH $\geq$ 10 observed in zip8e and nonzip1 is due to decomposition of BHQ3.

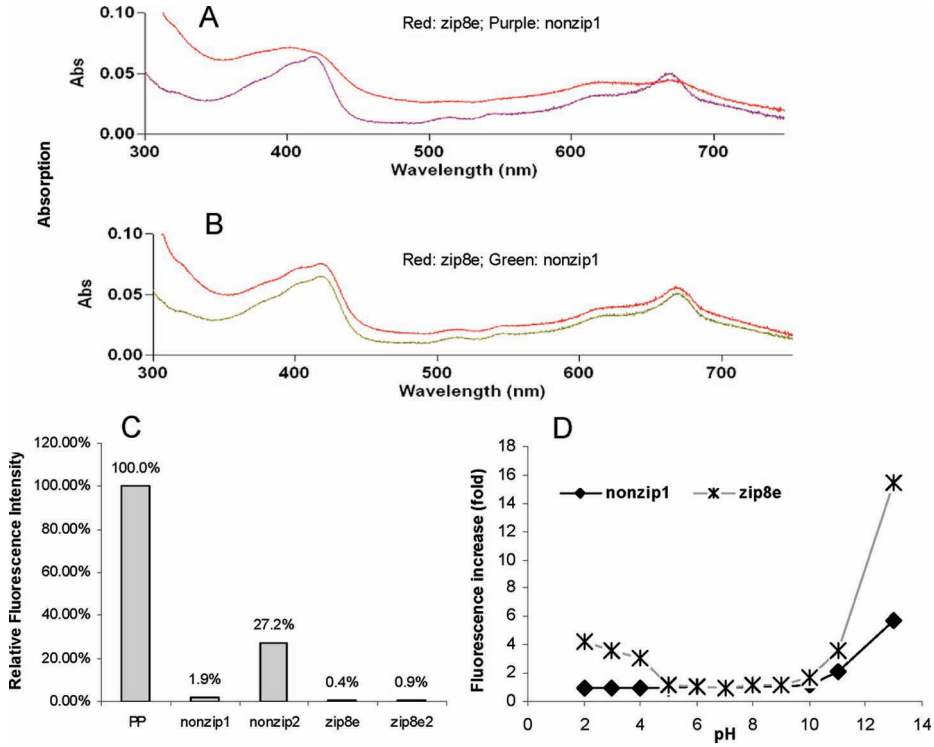

Figure 1. (A) Absorption spectra of zip8e and nonzip1 in (A) PBS buffer and (B) low-pH solution (pH = 2). (C) Relative fluorescence intensity of protease activatable probes (normalized to the fluorescence emission of PP). (D) The fluorescence stability of zip8e and nonzip1 in PBS buffer in the pH range 2−13.

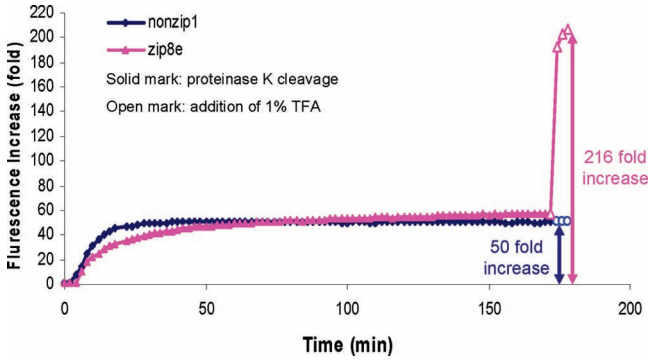

Figure 2. Comparison of the protease-mediated activation of ZMB and nonzipper probes: Cleavage kinetic profiles of probes depict increase in fluorescence after 3 h protease incubation and post TFA-induced disassociation.

Examining the protease-triggered activation of ZMB (Figure 2), we determined that the activation of ZMB is a two-step process. The first step is cleavage of the peptide linker and the second is dissociation of the zipper arms. Kinetic cleavage profiles of zip8e and nonzip1 were evaluated using Protease K to ensure complete proteolysis of the linker, and upon achieving stable fluorescence intensity, trifluoroacetic acid (TFA) was added. This decreased the pH to 2, neutralizing the polyanion arm and consequently causing dissociation of the zipper to produce maximum fluorescence. Both the nonzip1 and zip8e constructs were completely cleaved by Protease K in 3 h and produced similar maximum fluorescence. However, the fluorescence increases of these two probes were significantly different due to the enhanced quenching efficiency afforded by the zipper mechanism. As shown in Figure 2, nonzip1 resulted in a 50-fold fluorescence increase due to proteolysis with no further fluorescence increase after the addition of 1% TFA. In contrast, zip8e produced an overall 216-fold fluorescence increase. However, only a 57-fold fluorescence increase was observed 3 h after proteolysis and a 159-fold increase was contributed by forced dissociation of the zipper arms after the addition of 1% TFA. These results demonstrate that ZMB activation is a two-step process. When compared with the nonzip1 construct, ZMB offers much higher signal/background ratio after activation (216-fold vs 50-fold) due to a lower fluorescence background of intact ZMB, generated by zipper-enhanced fluorescence quenching.

This two-step activation creates a dilemma that is also observed in activatable cell-penetrating peptide probes in which the liberation of the peptide has a different mechanism on a much slower time scale (*15*). On one hand, a stable zipper conformation is necessary to achieve maximum quenching efficiency, which is critical for improving the probe sensitivity (by reducing the background fluorescence) and for creating the sequence-independent universal probe. On the other hand, if the zipper structure is too stable, it prevents or slows the prompt dissociation of the D- and Q-zipper arms upon target activation. This results in nonspecific diffusion of D from the target cells and diminishes the gain in probe selectivity. Hence, the optimal ZMB should have a high quenching efficiency balanced by rapid dissociation of the zipper arms after proteolysis.

Although zip8e provides near-maximum quenching efficiency (99.6%), its activation only produces a partial fluorescence increase (26%) from general proteolysis. In order to balance the quenching efficiency and activation, a collection of ZMBs with different zipper arm lengths (zip3e, zip4e, zip5e, zip6e) were synthesized (Supporting Information Figure S1 and Table S1). By comparing their fluorescence emission in PBS buffer, we found that the longer the zipper arm (polycation/ polyanion pair), the greater the quenching efficiency (Figure 3A). Upon

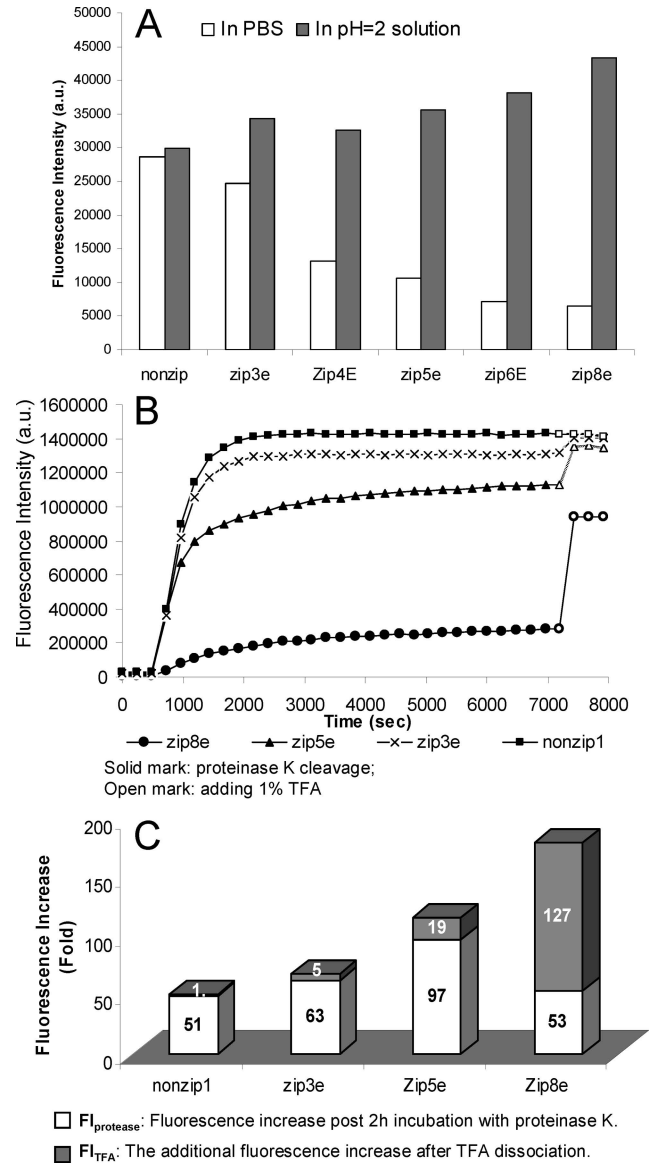

Figure 3. (A) Fluorescence emission of intact ZMBs in PBS and low pH condition (pH = 2). (B) Protease cleavage monitored by real time fluorescence. (C) $FI_{protease}$ and FI_{TFA} values for ZMBs and nonzipper controls.

adjusting the pH to 2, little to no fluorescence increase was observed in zip3e, suggesting that a zipper structure was not formed in this molecule, while a significant fluorescence increase, due to the low pH condition, was observed in zip4e, zip5e, zip6e, and zip8e, indicating that a zipper structure was formed in these molecules. The low pH conditions neutralize the polyanionic arm eliminating the electrostatic attraction between the zipper arms causing dissociation. This results in fluorescence release, as the D and Q are no longer electrostatically held together in close proximity.

As seen in Figure 3B, the activation of zip3e and zip5e was compared with that of nonzip1 and zip8e upon Proteinase K cleavage. Zip3e showed similar activation kinetics as nonzip1, further indicating that a 3-amino acid zipper arm length does not form a stable zipper. It had been previously observed that the 4-glutamate motif does not effectively attenuate the translocation of CPPs prior to proteolytic cleavage (*17*). Thus, these characteristics suggest that a stable zipper is formed when the ZMB is composed of more than 4 consecutive polycations and polyanions, resulting in enhanced fluorescence quenching efficiency and the two-step activation process. In Figure 3C, a

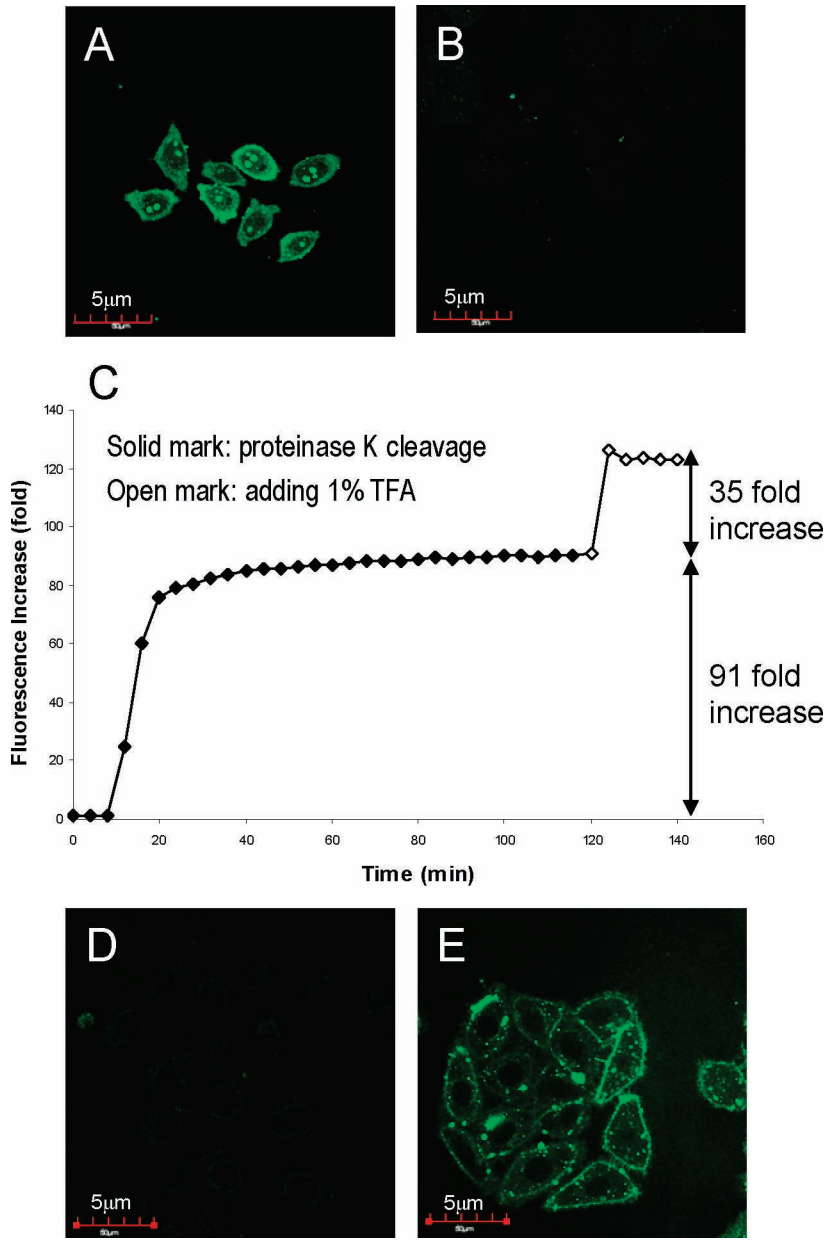

Figure 4. Confocal images of 5 μM (A) Fmoc-$_D$(rrrrrrrr)-K(FITC) and (B) Fmoc-$_D$(rrrrr)-K(FITC) in MT1 cells showing fluorescence in each case. (C) Activation kinetics of zip5e8r by Proteinase K in PBS. Confocal images of cell uptake of (D) nonzip1 and (E) zip5e8r at 30 min after cleavage by 3-day-old MT1 cell culture media.

97-fold fluorescence increase was seen in zip5e after proteolysis of the peptide linker ($FI_{protease}$), while only a 19-fold increase occurred after addition of TFA (FI_{TFA}). Thus, the dissociation of the zipper arms in zip5e is a much more efficient process than that of zip8e.

As all of the above fundamental studies were performed in PBS solution, we further evaluated the stability of the zipper arms in cell culture MEM media. Although the dissociation of the zipper arms is slightly increased in different buffered conditions, a 3−5% increase in fluorescence occurred; we assume that this buffer change will not greatly influence the kinetic profile of the zip PMBs (Supporting Information Figure S3).

Although zip5e has optimal cleavage and zipper arm dissociation rates, the practicality of a 5-amino acid polycation arm assisting in the internalization of the fluorophore is questionable. It has been reported that effective cell penetration requires at least 6 consecutive cationic amino acids (*23*). To validate this, *in vitro* confocal fluorescence microscopy was performed on Fmoc-$_D$(rrrrr)-K(FITC) and Fmoc-$_D$(rrrrrrrr)-K(FITC). As shown in Figure 4A,B, the 5-consecutive arginine cannot deliver the FITC into cells, whereas the 8-consecutive arginine showed a rapid uptake, within both the cytoplasm and nucleus after only 10 min incubation. This should address the limitation of nonspecific diffusion of the probe upon extracellular activation. Thus, by combining the optimal activation (cleavage and dissociation) of zip5e with the strong cell penetrating ability of 8-consecutive arginines, we designed an asymmetric ZMB with 8-consecutive arginines and 5-consecutive glutamates (zip5e8r): BHQ3-$_D$(eeeee)GPLGLA$_D$(rrrrrrrr)K(Pyro). This produces almost identical fluorescence quenching efficiency as zip5e (99.4% vs 99.3%), a similar rate of cleavage (2 h to completion) (Figure 4C) and comparable overall activation (72% vs 84%).

On the basis of these positive findings, zip5e8r was further evaluated in MT1 breast carcinoma cells *in vitro*, comparing the cell delivery of nonzip1 and zip5e8r after activation by 3-day-old cell incubated media. Although the peptide linker sequence is considered MMP7-specific (*12*), the old cell media

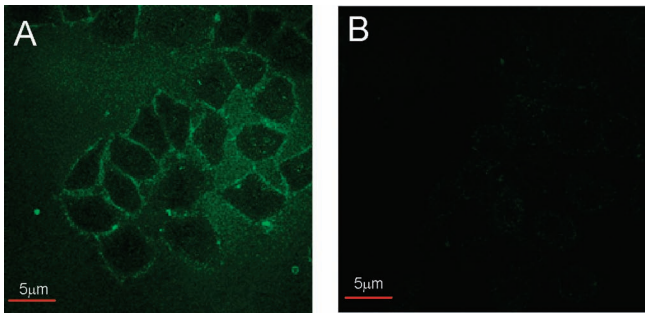

Figure 5. Confocal images comparing the background fluorescence in Pyro-ACPP (A) and zip5e8r (B).

contains a variety of different proteases, which might also lead to beacon activation. As shown in Figure 4D,E, the cleaved moiety of 8-consecutive arginine with Pyro (8r-Pyro) after zip5e8r activation accumulated inside the cells within 30 min, while the nonzip1 showed very weak uptake after activation. The improvement of zip5e8r ZMB over the corresponding nonquencher ACPP control, Pyro-ACPP, is shown in Figure 5 and Supporting Information Figure S5. By confocal imaging of the uptake of zip5e8r and Pyro-ACPP in fresh cell culture media and 3-day-old cell incubation media, we observed that the addition of a quencher significantly decreased the background signal, both before and after probe cleavage. Thus, ZMBs increased the resolution of activated probes and the contrast between the intact and activated beacon.

In summary, encoding a suitable zipper structure into protease-activatable probes significantly improves their functionality. First, by forming a stable zipper conformation, protease probes with different quenching efficiency can reach comparable maximum values (99.6% for zip8e and 99.1% for zip8e2). This effectively eliminates the peptide substrate sequence dependence of the quenching. Second, an optimal balance between high quenching efficiency and rapid activation (protease cleavage + zipper dissociation) can be achieved with 5-consecutive arginine paired with 5-consecutive glutamate (for both zip5e and zip5e8r). However, only the asymmetric zip5e8r with the extended polyarginine arm can facilitate rapid cell internalization. Thus, by incorporating an asymmetric zipper control, the quenching efficiency, activation, and delivery can all be optimized simultaneously, and the probe is no longer dependent on the specific peptide substrate sequence. Consequently, by simply switching the substrate sequences, the ZMB design can potentially be applied to a wide range of protease probe applications, with predictably similar functional performance.

This ZMB design has universal applications in targeted cancer fluorescence imaging/diagnostics, since in principle, any tumor biomarker can be targeted. Future advances may rely upon ZMBs targeted to novel early and reliable tumor markers that can discriminate malignant from benign lesions and detect micrometastases at distant sites. The application of ZMBs in cancer therapeutics is achievable by simply switching D to a fluorescent photosensitizer, such as pyropheophorbide. The ZMBs will then possess novel targeting capabilities for photodynamic therapy (PDT). With the activatable nature of ZMBs, another level of PDT selectivity should be achievable, improving the accuracy and reliability of this noninvasive therapeutic technique. Furthermore, with the fluorescent production upon activation of ZMBs, a "see and treat" approach in cancer therapeutics is also possible. The novelty of the ZMB construct is that it provides a universal design for any combination of Q and D or photosensitizer and any disease biomarker target. Thus, the applications of activatable molecular beacons in cancer diagnosis and therapy can be expanded with the incorporation of the "zipper" mechanism.

ACKNOWLEDGMENT

This work was supported by the Canadian Institute of Health Research, the Ontario Institute for Cancer Research through funding provided by the Government of Ontario, the Canadian Cancer Society Research Institute, and the Joey and Toby Tanenbaum/Brazilian Ball Chair in Prostate Cancer Research.

Supporting Information Available: Characterization of ZMB constructs, confirmation of protease K cleavage fragments of ZMBs, comparison of the fluorescence emission and kinetic profile of zip5e and zip8e in buffer solutions, comparison of ACPP vs ZMB in vitro after cleavage. This material is available free of charge via the Internet at http://pubs.acs.org.

LITERATURE CITED

(1) Weissleder, R., and Ntziachristos, V. (2003) Shedding light onto live molecular targets. *Nat. Med. 9*, 123–8.
(2) Weissleder, R., Tung, C. H., Mahmood, U., and Bogdanov, A. (1999) In vivo imaging of tumors with protease-activated near-infrared fluorescent probes. *Nat. Biotechnol. 17*, 375–8.
(3) McIntyre, J. O., Fingleton, B., Wells, K. S., Piston, D. W., Lynch, C. C., Gautam, S., and Matrisian, L. M. (2004) Development of a novel fluorogenic proteolytic beacon for in vivo detection and imaging of tumour-associated matrix metalloproteinase-7 activity. *Biochem. J. 377*, 617–628.
(4) Bullok, K., and Piwnica-Worms, D. (2005) Synthesis and characterization of a small, membrane-permeant, caspase-activatable far-red fluorescent peptide for imaging apoptosis. *J. Med. Chem. 48*, 5404–5407.
(5) Blum, G., von Degenfeld, G., Merchant, M. J., Blau, H. M., and Bogyo, M. (2007) Noninvasive optical imaging of cysteine protease activity using fluorescently quenched activity-based probes. *Nat. Chem. Biol. 3*, 668–677.
(6) Jaffer, F. A., Kim, D., Quinti, L., Tung, C., Aikawa, E., Pande, A. N., Kohler, R. H., Shi, G., Libby, P., and Weissleder, R. (2007) Optical visualization of cathepsin K activity in atherosclerosis with a novel, protease-activatable fluorescence sensor. *Circulation 115*, 2292–2298.
(7) Melancon, M. P., Wang, W., Wang, Y., Shao, R., Ji, X., Gelovani, J. G., and Li, C. (2007) A novel method for imaging in vivo degradation of poly(L-glutamic acid), a biodegradable drug carrier. *Pharm. Res. 24*, 1217–1224.
(8) Zhang, Z., Yang, J., Lu, J., Lin, J., Zeng, S., and Luo, Q. (2008) Fluorescence imaging to assess the matrix metalloproteinase activity and its inhibitor in vivo. *J. Biomed. Opt. 13*, 011006.
(9) Stefflova, K., Chen, J., Marotta, D., Li, H., and Zheng, G. (2006) Photodynamic therapy agent with a built-in apoptosis sensor for evaluating its own therapeutic outcome in situ. *J. Med. Chem. 49*, 3850–6.
(10) Chen, J., Stefflova, K., Niedre, M. J., Wilson, B. C., Chance, B., Glickson, J. D., and Zheng, G. (2004) Protease-triggered photosensitizing beacon based on singlet oxygen quenching and activation. *J. Am. Chem. Soc. 126*, 11450–1.
(11) Choi, Y., Weissleder, R., and Tung, C. (2006) Selective antitumor effect of novel protease-mediated photodynamic agent. *Cancer Res. 66*, 7225–7229.
(12) Zheng, G., Chen, J., Stefflova, K., Jarvi, M., Li, H., and Wilson, B. C. (2007) Photodynamic molecular beacon as an activatable photosensitizer based on protease-controlled singlet oxygen quenching and activation. *Proc. Natl. Acad. Sci. U.S.A. 104*, 8989–94.
(13) Gabriel, D., Campo, M. A., Gurny, R., and Lange, N. (2007) Tailoring protease-sensitive photodynamic agents to specific disease-associated enzymes. *Bioconjugate Chem. 18*, 1070–1077.
(14) Lo, P., Chen, J., Stefflova, K., Warren, M. S., Navab, R., Bandarchi, B., Mullins, S., Tsao, M., Cheng, J. D., and Zheng,

G. (2009) Photodynamic molecular beacon triggered by fibroblast activation protein on cancer-associated fibroblasts for diagnosis and treatment of epithelial cancers. *J. Med. Chem. 52*, 358–368.

(15) Jiang, T., Olson, E. S., Nguyen, Q. T., Roy, M., Jennings, P. A., and Tsien, R. Y. (2004) Tumor imaging by means of proteolytic activation of cell-penetrating peptides. *Proc. Natl. Acad. Sci. U.S.A. 101*, 17867–72.

(16) Goun, E. A., Shinde, R., Dehnert, K. W., Adams-Bond, A., Wender, P. A., Contag, C. H., and Franc, B. L. (2006) Intracellular cargo delivery by an octaarginine transporter adapted to target prostate cancer cells through cell surface protease activation. *Bioconjugate Chem. 17*, 787–96.

(17) Watkins, G. A., Jones, E. F., Scott Shell, M., VanBrocklin, H. F., Pan, M., Hanrahan, S. M., Feng, J. J., He, J., Sounni, N. E., Dill, K. A., Contag, C. H., Coussens, L. M., and Franc, B. L. (2009) Development of an optimized activatable MMP-14 targeted SPECT imaging probe. *Bioorg. Med. Chem. 17*, 653–9.

(18) Zhang, M., Zhang, Z., Blessington, D., Li, H., Busch, T. M., Madrak, V., Miles, J., Chance, B., Glickson, J. D., and Zheng, G. (2003) Pyropheophorbide 2-deoxyglucosamide: a new photosensitizer targeting glucose transporters. *Bioconjugate Chem. 14*, 709–14.

(19) Knight, C. G., Willenbrock, F., and Murphy, G. (1992) A novel coumarin-labelled peptide for sensitive continuous assays of the matrix metalloproteinases. *FEBS Lett. 296*, 263–6.

(20) Welch, A. R., Holman, C. M., Browner, M. F., Gehring, M. R., Kan, C. C., and Van Wart, H. E. (1995) Purification of human matrilysin produced in *Escherichia coli* and characterization using a new optimized fluorogenic peptide substrate. *Arch. Biochem. Biophys. 324*, 59–64.

(21) Hamamoto, K., Kida, Y., Zhang, Y., Shimizu, T., and Kuwano, K. (2002) Antimicrobial activity and stability to proteolysis of small linear cationic peptides with D-amino acid substitutions. *Microbiol. Immunol. 46*, 741–9.

(22) Gammon, S. T., Villalobos, V. M., Prior, J. L., Sharma, V., and Piwnica-Worms, D. (2003) Quantitative analysis of permeation peptide complexes labeled with Technetium-99m: chiral and sequence-specific effects on net cell uptake. *Bioconjugate Chem. 14*, 368–76.

(23) Mitchell, D. J., Kim, D. T., Steinman, L., Fathman, C. G., and Rothbard, J. B. (2000) Polyarginine enters cells more efficiently than other polycationic homopolymers. *J. Pept. Res. 56*, 318–25.

BC900207K

Photodynamic Molecular Beacons in Breast Cancer Vertebral Metastases: Imaging Validation of Beacon Specificity

Tracy W. Liu[1,2], Margarete Akens[3], Juan Chen[2], Lisa Wise-Milestone[3], Brian C. Wilson[1,2], Gang Zheng[1,2]

[1]Department of Medical Biophysics, University of Toronto, Canada; [2]Ontario Cancer Institute, University Health Network, Canada; [3]Sunnybrook Health Science Centre, Canada.

Running Title: Photodynamic molecular beacons for vertebral metastases

Keywords: Breast cancer, Metastasis/metastasis genes/metastasis models, vertebral metastases, MMP, activatable probe.

Gang Zheng
5-363 101 College St.
Toronto, Canada
M5G 1L7
416-581-7666 (Primary)
416-581-7667 (Fax)
gang.zheng@uhnres.utoronto.ca

word count: 3, 969

total number of figures and tables: 6

Statement of Translational Relevance:

Vertebral metastases are a major clinical problem in breast cancer patient management. Current therapies have significant limitations due to the high associated risk of damaging the spinal cord. Here we demonstrate the potential of using MMP-triggered photodynamic molecular beacons to achieve high specificity against vertebral metastases. Explicitly, beacons achieve what current photosensitizers lack, the ability to target intravertebral metastatic tumours with minimal uptake in the spinal cord. This work has the potential to aid in the clinical translation of photodynamic molecular beacons, specifically in the photodynamic treatment of spinal metastases. Furthermore, we believe the beacon's remarkable ability to differentiatiate metastatic versus critcal tissues provides a wide range of clinical implications such as tools for fluorescence image-guided surgical resection, surgical bed clean up or for in adjuvant therapy with vertebroplasty.

Abstract

Purpose: The vertebral column is the most common site of breast cancer metastases, where overexpression of matrix metalloproteinases (MMPs) promotes the spread of cancer. Current therapies for managing vertebral metastases have significant limitations due to high associated risk of spinal cord damage. An attractive alternative is photodynamic therapy providing non-invasive and site-selective treatment. However, current photosensitizers are limited by their non-specific accumulation. Photodynamic molecular beacons ($PP_{MMP}B$), activated by MMPs, offer another level of PDT selectivity and image-guidance preserving criticial tissues, specifically the spinal cord.

Experimental Design: $PP_{MMP}B$ activation was validated *in vitro* using human MT-1 metastatic breast cancer cells. Preliminary *in vivo* activation was demonstrated in MT-1 xenografts in athymic mice. A scrambled beacon with a non-cleavable peptide linker was

used as a control. For a relevant preclinical model, MT-1 cells were injected intra-cardially to establish vertebral metastases in athymic rats. $PP_{MMP}B$ activation within the spinal column was assessed 2, 4, 12 and 24 h after intravenous injection and further compared in tumor-bearing *versus* healthy animals 2 and 4h post injection. The dose of $PP_{MMP}B$ was 3mg/kg bodyweight.

Results: *In vitro* studies confirm the specific activation of $PP_{MMP}B$ in MT-1 cells. *In vivo* experiments demonstrate specific activation of $PP_{MMP}B$ in MT-1 xenografts, using systemic and intratumoral injections. Using a clinically-relevant metastatic model, fluorescent imaging confirmed the specific activation of $PP_{MMP}B$ by vertebral metastases.

Conclusions: As a first step, we validate that the metastasis-selective mechanism of $PP_{MMP}Bs$ can specifically image breast cancer vertebral metastases, thereby differentiating tumor and healthy tissue.

Introduction

Metastatic spread of tumor cells is the most devastating attribute of cancer and is often the cause of mortality. Due to the unique microenvironment of the bone, it is the most common site of distant metastases from cancers of the breast, lung, kidney, thyroid and prostate.(1) The bone provides a fertile environment for the growth of cancer and promotes the aggressive behavior of tumor cells, since the mineralized bone matrix houses many growth factors, bone-destroying osteoclasts and bone-forming osteoblasts.(1) Approximately 85% of breast cancer patients with metastatic disease will develop bone metastases, in which the vertebral column is the most common site for metastatic formation.(2, 3) Matrix metalloproteinases (MMPs) are a family of

structurally-related, zinc-dependent endopeptidases implicated in the invasion and metastasis of cancer through the degradation of the basement membrane and collagen-rich extracellular matrix.(4-7) Furthermore, MMPs are exquisite regulators of the tumor microenvironment by virtue of their ability to process many biological modulators, such as cytokines and growth factors within the bone matrix.(4-6)

Breast cancer spinal metastases are predominantly osteolytic (bone destructive), which is associated with an increase in osteoclast activity.(1) Metastasis disrupts the dynamic balance between bone resorption by osteoclasts and bone formation by osteoblasts, inducing a vicious cycle whereby tumor cells reprogram osteoclasts, leading to osteolysis and promotion of tumor growth.(1, 2) MMPs play a vital role in signaling cascades involved in metastatic growth, and their upregulation leads to the processing of many growth factors, including TGF-β,(8) IGFs,(9) E-caderin(10) and RANKL(11) that are all essential for metastatic tumor progression within the vertebral body.(7, 12, 13) MMPs themselves also destroy healthy tissue, particularly in the bone, since the matrix is composed primarily of mineralized fibrillar type I collagen,(7) a main substrate of many MMPs. The upregulation of MMPs is thus critically involved in the destruction of the delicate balance between bone formation and degradation, reducing bone integrity (Figure 1A).(1, 2) Hence, MMPs not only aid the spread of tumor cells to distant sites, but are also involved in the local dissolution of the vertebral body and promote tumor progression within the vertebrae.

The resulting osteolysis causes bony pain, vertebral pathological fractures, progressive deformity, hypercalcemia and spinal instability.(1, 2) Patients with spinal metastases have a high risk of spinal cord compression, resulting in motor dysfunction,

neurological compromise and an overall poor prognosis.(1, 2) The associated 5-year survival rate in patients with spinal metastases is below 20% compared to a 5-year survival rate over 85% in patients with early stage breast cancer.(14) Regardless of the symptoms, all patients suffering from spinal metastases experience a substantial decrease in their quality of life. Surgery and radiation therapy are the main treatment options for these patients. Surgical treatments, however, carry a high risk of morbidity due to the proximity of the spinal cord, while radiation therapy is limited to a level far below the optimal therapeutic dose because of the low tolerance of the spinal cord.(15) Clinical studies of radiotherapy have reported recurrence of symptoms, and pain relief is not experienced until at least 3 months after treatment.(16) Lastly, although pain relief and, in part, tumor regression are addressed by radiation treatment, spinal instability is not. Therein lies the need for improved therapies that specifically targets metastatic tumor cells while preserving the spinal cord to address pain relief, tumor regression and mechanical instability of the spine.

PDT is an approved cancer treatment modality that destroys target cells when light activates a non-toxic photosensitizer (PS) to generate cytotoxic excited-state (singlet) oxygen.(17-19) It has several potential advantages over current cancer treatments due to its minimally-invasive nature, selectivity, ability to treat patients with repeated doses without initiating resistance or exceeding total-dose limitations, fast healing that results in little or no scarring, the ability to administer in an outpatient setting, minimal associated side effects and lack of contraindication with other modalities.(17-19) We have previously proposed and reported several preclinical studies on the concept of using PDT for destroying spinal metastases, particularly to debulk

lesions as an adjuvant to vertebroplasty or kyphoplasty in order to mechanically stabilize weak or fractured vertebrae:(20-25) These surgical procedures involve injection of a plastic compound or placement of an inflatable balloon into the vertebral body, which is often limited by the space-occupying tumor mass. We have shown that, not only can PDT (using the clinical photosensitizer Visudyne®) ablate spinal metastatic tumors,(20) but unexpectedly it also enhances vertebral mechanical stability.(24, 25) However, current photosensitizers are limited by their non-specific accumulation in normal tissues: e.g., Visudyne has non-specific uptake in the spinal cord limiting the therapeutic window which, in turn, reduces the aggressiveness of treatment in order to stay well within safe dose limits.(20, 21) Clearly, preservation of spinal cord structure and function is critical in the management of vertebral metastases.

Photodynamic molecular beacons were introduced by us to provide an additional mechanism of selectivity in PDT over and above those due to photosensitizer and light targeting.(26) This is illustrated in Figure 1B. The beacons comprise a photosensitizer and a quencher moiety, linked, in the present case, by a MMP-cleavable peptide ($PP_{MMP}B$). They remain 'optically silent', i.e. photodynamically inactive, until transformed into an activated state through cleavage of the linker, upon which both the PDT activity and PS fluorescence are restored, the latter providing the potential for real-time image guidance.(26) Furthermore, as $PP_{MMP}Bs$ are only activated in the presence of these secreted tumor-specific proteases, normal tissues, including the spinal cord, should remain relatively protected.(26) One concern is that uptake of activated $PP_{MMP}Bs$ by the spinal cord may occur if activated beacons are allowed sufficient time to diffuse from the tumor to normal tissues. Here, as a first step in implementing $PP_{MMP}Bs$ as a therapeutic

strategy for the management of vertebral metastases, we validate that the metastasis-selective mechanism of PP_{MMP}Bs can specifically target breast cancer vertebral metastases, thereby differentiating tumor and healthy tissue.

Materials and Methods

Study Design

PP_{MMP}B activation was validated *in vitro* using the human MT-1 metastatic breast cancer cell line that express MMPs. Preliminary *in vivo* activation was demonstrated in MT-1 xenografts grown subcutaneously on the flank of athymic mice. A scrambled beacon, $PP_{scrambled}$B, in which the peptide linker sequence is not cleavable by MMPs,[20] was used to validate the specific activation of PP_{MMP}B by the MT-1 cells. As a relevant preclinical model of vertebral metastases, MT-1 cells were injected intra-cardially to establish metastases in athymic rats. The activation of PP_{MMP}B within the spinal column was assessed at each of 2, 4, 12 and 24 h after intravenous injection of PP_{MMP}B. PP_{MMP}B activation was further compared in tumor-bearing *versus* healthy animals, at each of 2 and 4h post injection. The fixed dose of PP_{MMP}B was 3mg per kg bodyweight, equivalent to that using Visudyne in previous studies with this model (20).

PP_{MMP}B Synthesis

The PP_{MMP}B consists of the photosensitizer Pyropheophorbide-α (PS) and black hole quencher 3 (Q), linked by the amino acid sequence GPL*GL*ARK, which is an MMP-cleavable peptide: italics indicate the cleavage site. It was synthesized as described previously.(26) $PP_{scrambled}$B comprises the same PS and Q but with a linker sequence,

tsgpnqeqk, composed of d-amino acids that has been shown not be cleaved by MMPs.(27)

Cells

MT-1 cells, a human metastatic breast cancer cell line, were kindly provided by Dr. O. Engebraaten, Norwegian Radium Hospital, Norway. Cells were grown and maintained in Roswell Park Memorial Institute (RPMI) 1640 media supplemented with 10% fetal bovine serum at 37 °C in an atmosphere of 5% CO_2 in a humidified incubator. The MT-1 cells were stably infected with a double-fusion plasmid (luciferase and green flurescent protein, GFP) kindly provided by Dr. Joseph Wu (Stanford University) and a lentivirus kindly provide by Dr Ren-Ke Li, (University of Toronto). The expression of GFP and luciferase provides a means to identify the cells and assess their viability.[22]

In vitro model

In vitro activation of $PP_{MMP}B$ was evaluated by both confocal microscopy and flow cytometry. $PP_{MMP}B$ (2nmol) or $PP_{scrambled}B$ (2nmol) were first dissolved in 2% dimethyl sulfoxide, DMSO (Sigma Aldrich), and 0.025% Cremophore®. The solutions were then diluted with the culture medium to a final concentration of 10μM (molecular weight of the $PP_{MMP}B$ is 1856 g/mol). 2×10^4 cells in 0.4 mL of culture medium per well were seeded in Nunc Laboratory-TekII-CC2 8-well chamber slides and incubated for 2 days at 37 °C under 5% CO_2 in a humidified incubator to grow to 80% confluency. $PP_{MMP}B$ activation after 6h incubation of MT-1 cells was assessed using a laser scanning confocal microscope (Olympus FluoView 1000: 633 nm excitation, > 650 nm detection). For this, $2x10^5$ cells in 2 mL of medium per well were inoculated in 6-well plates and incubated for 2 days at 37°C under 5% CO_2 in a humidified incubator. The cells were

then incubated with 1mL of $PP_{MMP}B$ or $PP_{scrambled}B$ solution (10μM) for 1 and 6h respectively, at 37°C under 5% CO_2. The beacon solution was then removed after above incubation times and assessed by HPLC-MS to confirm the beacon cleavage. The cells were trypsinized from the well plates and transferred to a 15 mL centrifuging tube containing 2 mL PBS. The cells were centrifuged at 1000 rpm for 6 min and the PBS was removed. This rinsing procedure was repeated 3 times. The cells were fixed by a 2% paraformaldehyde solution for 10 min, after which they were centrifuged and rinsed twice with PBS. The fluorescence intensities of the cells were measured by flow cytometry (CytomicsFC 500, Beckman Coulter, CA, USA: 633 nm excitation, 660-690 nm detection). The maximum cell count was approximately 10,000 in each sample.

In vivo xenograft model

All animal studies were carried out under institutional approval (University Health Network, Toronto, Canada). Adult athymic female nude mice were inoculated subcutaneously with $1x10^6$ MT-1 cells in 200μL of media in both the left and right flanks for intratumoural injection studies of $PP_{MMP}B$. To evaluate the activation of $PP_{MMP}B$ by a systemic injection, mice were inoculated similarly only on the right flank. Animals were maintained in pathogen-free conditions in autoclaved microisolator cages. After 2 weeks, by which time the tumors were 5-10 mm in diameter, the mice were fed a low-fluorescence diet (Harlan Tekland) for 4 days to reduce the autofluoresence background. A 2mg/kg dose of $PP_{MMP}B$ or $PP_{scrambled}B$ was formulated in 30 μL of aqueous solution with 2% DMSO and 0.5% Tween-80. Under general anesthesia (isofluorane in oxygen), a 27G needle was used to inject this in multiple locations in the tumor to improve the distribution. A 2mg/kg intravenous injection (tail vein) of $PP_{MMP}B$ was formulated in

150uL of aqueous solution with 2% DMSO and 0.5% Tween-80. Whole-body *in vivo* fluorescence imaging was performed before and at multiple time points after injection (Maestro^{TM}, CRi: 650 nm excitation, ≥ 700 nm detection, autoexposure integration time].

Ex vivo xenograft studies

MT-1 tumors harvested from mice 24h following intratumor injections of beacon and were snap-frozen in liquid nitrogen and stored at -70 °C. Frozen sections (10 μm) were cut on a cryostat. After 5 min at room temperature the slides were immersed in PBS for another 5 min, then dried, and 4 μL of mounting solution with DAPI, 4',6-diamidino-2-phenylindole (Vector laboratories. Inc.), was added as a nuclear stain. The sections were covered by a cover slip and imaged by confocal microscopy similar to the *in vitro* studies above.

In vivo vertebral metastases model

Female 5–6 week old athymic rats (rnu/rnu; Harlan Sprague Dawley, Indianapolis, IN, USA) were used as a model to mimick vertebral metastatic spread. The activation of $PP_{MMP}B$ was compared in the spinal column in tumor-bearing and healthy animals. Under general inhalation anesthesia (isofluorane in oxygen) MT-1 cells were injected intra-cardially at a concentration of 2×10^6 in 0.2 ml of RPMI1640 media. Fourteen days later *in vivo* bioluminescence imaging was performed as follows to confirm the establishment of metastases. Luciferin (Xenogen Corp., MA, USA) was dissolved in 0.9% NaCl at a concentration of 30 mg/ml and a single dose of 60 mg/kg was injected intra-peritoneally into anaesthetized animals, which were immediately placed ventrally in a whole-body bioluminescence imager (IVIS Spectrum: Caliper Life Sciences, CA, USA), integrating the counts over 30 s (Fig. 2A). Following this, 3mg/kg

of $PP_{MMP}B$ in 2% DMSO, 0.5% Tween80 was injected through the tail vein and, at each time point above, cohorts were euthanized by pentobarbital overdose.

Ex vivo vertebral metastases studies:

At the time of necroscopy in these animals, the T13- L4 vertebrae were harvested intact, transferred to PBS and immediately cut in the sagittal plane using a low-speed precision saw (IsoMet, Buehler, Illinois). $PP_{MMP}B$ activation by MT-1 vertebral tumors was assessed by confocal microscopy of the cut surface (633 nm excitation, > 650nm detection) at 10X magnification. These images were overlaid by corresponding GFP images from the MT-$1^{luc/GFP}$ cells (488 nm excitation, >520 nm detection), in order to evaluate the specific activation of $PP_{MMP}B$ *in vivo* by MT-1 metastases. Using commercial software (Olympus FluoView™ FV1000), the degree of co-localization of $PP_{MMP}B$ and MT-1 metastatic cells within the vertebral column was assessed by calculating the Pearson coefficient between the two fluorophores (activated $PP_{MMP}B$ and GFP), with -1 representing no overlap and +1 representing 100% concordance of localization. $PP_{MMP}B$ activation was quantified in these samples using the Maestro imaging system (650 nm excitation, ≥ 700 nm detection, autoexposure integration time), normalizing the total fluorescence signal within a defined region of interest (ROI) by the exposure time and the ROI area. The values used were based on the mid-sagittal images of the fluorescence within the vertebral body and the spinal cord, and the difference between these was compared using a Student t-test. To confirm metastatic formation within the vertebral column, the spines were then fixed in 10% buffered formalin, decalcified, sectioned (10 µm) and stained either with H&E or immunhistochemically using a mouse-anti-human epidermal growth factor receptor (hEGFr) antibody (Zymed®,

Laboratories Inc., San Francisco, CA, USA). This antibody does not cross react with rat tissues, enabling specific visualization of the metastatic human breast cancer cells within the rat vertebral bone and bone marrow compartments (Figure 2B).

Results

The *in vitro* specific activation of $PP_{MMP}B$ by MT-1 cells was compared with that of the scrambled beacon ($PP_{scrambled}B$) in which the linker was not MMP cleavable, as illustrated by confocal fluorescence microscopy: Figures 3A and B. HPLC-MS of the culture media following incubation with the cells shows 2 peaks that correspond to the fragments Pyro-GPLG and LARK-BHQ3 only with $PP_{MMP}B$ (Fig. S1), corresponding to the expected MMP cleavage site. Examples of flow cytometry to quantify the fluorescence intensity of $PP_{MMP}B$ and $PP_{scrambled}B$ in the cells incubated for different times are shown in Figure 3C. At all time points the fluorescence intensity was 5- to 10-fold higher in cells incubated with $PP_{MMP}B$ than with the scrambled beacon ($p< 0.001$). The distributions and shape of the cells are largely homogenous after incubation with the beacons, suggesting minimal toxicity (Fig. S2).

The activation of $PP_{MMP}B$ *in vivo* was first examined in subcutaneous MT-1 xenografts, following i.v. administration of 2mg/kg $PP_{MMP}B$, monitoring the fluorescence following cleavage by whole-body imaging. A strong fluorescence signal localized within the tumor was seen in both experimental animals (Figure 4A), demonstrating $PP_{MMP}B$ activation in the tumor. To further validate the *in vivo* MMP specificity, mice bearing tumors on both flanks were injected intratumorally with 2mg/kg of either $PP_{MMP}B$ (left) or $PP_{scrambled}B$ (right) and followed over time. Initially, little fluorescence

was observed in either tumor. However, at 6h a 10-fold increase in tumor fluorescence was observed with $PP_{MMP}B$ compared with $PP_{scrambled}B$, the latter showing minimal change in fluorescence (Figure 4B). Even after 24 h, confocal images of frozen sections of harvested tumors confirmed that fluorescence was only detectable in tumors injected with $PP_{MMP}B$ (Figure 4C).

Although these results are promising, evaluation of $PP_{MMP}B$ specific activation in veretebral metastases is needed to validate the PDT beacon concept for this particular clinical application. Following intracardiac injection of MT-1 cells, metastatic spread to the spine was seen in all animals using bioluminescent imaging. *Ex vivo* fluorescence imaging of the sagitally-cut spine over 24 h evaluated $PP_{MMP}B$ activation in vertebral metastases. As shown in Figure 5, the highest fluorescence signal was between 2 and 4 h and then significantly decreased ($p < 0.05$) at 12 and 24 h. Importantly, no fluorescence signal from activated beacons was detected above background within the spinal cord at any time point (Fig. 5B and Fig. S3). Weak fluorescence was observed within the intervertebral discs (Fig. 5A). The strongest fluorescence was within the vertebral body, where metastases most commonly form. At all imaging time points, the fluorescence intensity was 6 to 9-fold higher in the vertebral body versus the spinal cord ($p<0.05$) (Fig. 5B), demonstrating that $PP_{MMP}B$ activation is substantively confined to sites where vertebral metastases develop, with rapid onset of beacon activation after administration. Thus, either the beacon is not significantly taken up in or activated by the spinal cord or, at least over the time period of observation, there is no significant diffusion of cleaved $PP_{MMP}B$ activated by tumors (local or distant) into the spinal cord.

To ensure that $PP_{MMP}B$ activation was a result of the vertebral metastases expressing MMPs and not due to normal bone tissues, spines from tumor-bearing and healthy animals were imaged *ex vivo* at 2 and 4 h after i.v. administration of $PP_{MMP}B$. No fluorescence was observed in the spinal cord in either case. Under confocal microscopy, in which the unquenched beacon fluorescence was overlaid with the GFP signal of the cells, sites with positive GFP showed detectable activation (Figs 6A,B), whereas no activation was detected in the healthy animals (Figs 6C,D). Furthermore, no $PP_{MMP}B$ activation was seen within the spinal cord. The Pearson coefficients for the degree of overlap between $PP_{MMP}B$ activation and MT-1 vertebral tumors (Figs. 6 A, B and S4) were 0.76 and 0.68 at 2 and 4 h post injection, respectively. This was not applicable in the healthy animal cohort, since no signal was detected in either imaging channel (tumor or cleaved beacon).

Discussion

These data, while limited in the number of animals and time points examined, demonstrate that specific activation (enzymatic cleavage resulting in unquenching of the photosensitizer fluorescence) of $PP_{MMP}Bs$ is mediated by breast cancer vertebral metastases that express MMPs. The *in vitro* studies confirm this specific activation by the MT-1 breast cancer cells. The *in vivo* experiments in MT-1 xenografts demonstrate specific activation of $PP_{MMP}B$ by these tumors, using both systemic (i.v.) and intratumoral injection of the beacon. In the more clinically-relevant metastatic model, fluorescent imaging also confirmed tumor-specific activation of $PP_{MMP}B$. There are, however, limitations with this model. The attenuation of the fluorescent signal by the

overlying bone and soft tissue confounds quantitative *in vivo* imaging to determine the activation kinetics. Nevertheless, this could be determined by imaging the sectioned vertebrae *ex vivo*, albeit at only select time points, and showed that the beacon can reach and target the intravertebral tumor tissue. In addition, it remained inactive (uncleaved) within the spinal cord, which is the critical dose-limiting tissue. Although in this initial study we have not directly tested the photodynamic efficacy of the cleaved beacon against the tumor tissue, previous studies of a variety of PDT beacons in tumor xenograft models(26) have shown that this tracks with the fluorescence characteristics, as would be expected from the photophysics. It may be anticipated then that $PP_{MMP}B$ is able to serve as both a vertebral metastases-specific imaging agent and a directed PDT agent. Direct studies of the PDT effect are in progress, although a second limitation of the intracardiac-injection metastatic model is that the animals survive for only a few weeks(20) due to widespread disease, so that long-term treatment responses cannot be evaluated. Due to the small size of the animals, evaluation of the PDT effect due to an intratumoral injection of $PP_{MMP}B$ within the vertebrae is not possible.

There are a number of potential applications of PDT beacons in the treatment of patients with vertebral metastases. Surgical debulking is currently a main treatment option, but recurrence is common due to incomplete resection. The strong fluorescence signal and specificity of the beacon could then enable intra-operative image guidance to increase the completeness of resection and to aid in the intraoperative detection of small metastatic lesions that are otherwise not visible. Thereby, the risk of recurrence would be reduced. This is also analogous to fluorescence image-guided tumor resection in other organs.(17, 28-33) Furthermore, original fluorescent protease activatable probes were

developed to differentiate tumor versus healthy tissue better defining surgical margins. Thus, the initial *in vivo* and clinical application of beacons was intended for fluorescence image-guided tumor resection.(18, 34-38). We have demonstrated tumor-specific activation for both systemical and local administration in the tumor xenografts. Intratumoral injection was not technically feasible in the vertebral metastasis model due to the size limitation, but this will not be the case in patients. It is encouraging that activation occurs fairly rapidly, so that the beacon could be administered shortly before or during surgery, assuming comparable activation kinetics in humans after a local injection at the tumor site.

In the second aspect, since pyropheophorbide-α is a potent PDT agent(26, 27) in addition to being a fluorescence marker, PDT could be used as means to 'clean up' the surgical bed following resection, as has been used in gliomas with conventional photosensitzers.(28, 39) The high degree of quenching in the intact beacon (>99%) and the tumor specificity of activation are then distinct advantages, by markedly reducing the risk of collateral damage to normal tissues that are within range of the photoactivating light. Thus, PDT treatment of the entire surgical bed post-resection could result in the eradication of any residual tumor mass and microscopic metastatic deposits, while preserving normal tissues. Furthermore, based upon the confocal imaging of tumor cell GFP and beacon activation in vertebral metastases (Figs. 6Aiv and 6Biv), there is evidence of beacon uptake by tumor stroma as well as by the tumor cells themselves. This is not too surprising, since it is known that MMPs are also secreted by tumor stroma.(4, 5) This multi-compartment targeting provides a further means to interrupt the signaling between the stroma and adjacent cancer cells by identifying cells hijacked by

the tumor to promote osteolysis. Hence, eradication of the tumor microenvironment would result in further synergistic effects.

Beacons such as $PP_{MMP}B$ may be a key component in the use of PDT as a new, minimally-invasive, safe and effective therapy for the management of patients with spinal metastases when used, for example, as an adjuvant to minimally-invasive surgical techniques such as vertebroplasty or kyphoplasty for mechanical stabilization.(20, 22, 23) We have recently strated a Phase I clinical trial with the clinically-approved photosensitzer Visudyne (QLT Inc, Vancouver, BC, Canada), in which the objective is to debulk the intravertebral space-occupying tumor mass that often impedes these surgical approaches. However, based on preclinical studies(20, 21), the therapeutic window is likely to be limited by the non-specific uptake of the photosensitizer by healthy tissues, including the spinal cord, which will restrict the drug and light doses that can be used safely. $PP_{MMP}B$ potentially addresses this limitation. To this end, as mentioned above, we are currently evaluating the therapeutic window of $PP_{MMP}B$ PDT and the effect of $PP_{MMP}B$ PDT-induced tumor destruction within the vertebrae.

In summary, we have demonstrated the specific activation of $PP_{MMP}B$ by MMP-expressing vertebral metastases in a relevant preclinical model illustrating defined kinetics and the ability to target intravertebral metastatic tumors with minimal uptake or activation in the spinal cord. This is a first step in the further development of such beacons and their potential translation into useful clinical tools for a range of applications.

Acknowledgements

This work was supported by the Canadian Institutes of Health Research, DOD BCRP Predoc Award W81XWH-10-1-0115, and Joey and Toby Tanenbaum/Brazilian Ball Chair in Prostate Cancer Research. Partial support was provided by the Princess Margaret Hospital Foundation and the Ontario Ministry of Health & Long Term care.

References

1. Mundy GR. Metastasis to bone: causes, consequences and therapeutic opportunities. Nat Rev Cancer. 2002;2:584-93.
2. Siclari VA, Guise TA, Chirgwin JM. Molecular interactions between breast cancer cells and the bone microenvironment drive skeletal metastases. Cancer metastasis reviews. 2006;25:621-33.
3. Kingsley LA, Fournier PG, Chirgwin JM, Guise TA. Molecular biology of bone metastasis. Mol Cancer Ther. 2007;6:2609-17.
4. Brinckerhoff CE, Matrisian LM. Matrix metalloproteinases: a tail of a frog that became a prince. Nature reviews. 2002;3:207-14.
5. Kessenbrock K, Plaks V, Werb Z. Matrix metalloproteinases: regulators of the tumor microenvironment. Cell.141:52-67.
6. Woodward JK, Holen I, Coleman RE, Buttle DJ. The roles of proteolytic enzymes in the development of tumour-induced bone disease in breast and prostate cancer. Bone. 2007;41:912-27.
7. Guise TA. Breaking down bone: new insight into site-specific mechanisms of breast cancer osteolysis mediated by metalloproteinases. Genes Dev. 2009;23:2117-23.
8. Yu Q, Stamenkovic I. Transforming growth factor-beta facilitates breast carcinoma metastasis by promoting tumor cell survival. Clin Exp Metastasis. 2004;21:235-42.
9. Kasper G, Reule M, Tschirschmann M, Dankert N, Stout-Weider K, Lauster R, et al. Stromelysin-3 over-expression enhances tumourigenesis in MCF-7 and MDA-MB-231 breast cancer cell lines: involvement of the IGF-1 signalling pathway. BMC Cancer. 2007;7:12.
10. Noe V, Fingleton B, Jacobs K, Crawford HC, Vermeulen S, Steelant W, et al. Release of an invasion promoter E-cadherin fragment by matrilysin and stromelysin-1. J Cell Sci. 2001;114:111-8.
11. Lynch CC, Hikosaka A, Acuff HB, Martin MD, Kawai N, Singh RK, et al. MMP-7 promotes prostate cancer-induced osteolysis via the solubilization of RANKL. Cancer Cell. 2005;7:485-96.
12. Egeblad M, Werb Z. New functions for the matrix metalloproteinases in cancer progression. Nat Rev Cancer. 2002;2:161-74.
13. Page-McCaw A, Ewald AJ, Werb Z. Matrix metalloproteinases and the regulation of tissue remodelling. Nature reviews. 2007;8:221-33.
14. American Cancer Society. Breast Cancer Facts & Figures 2009-2010. Atlanta: American Cancer Society I.
15. Finn MA, Vrionis FD, Schmidt MH. Spinal radiosurgery for metastatic disease of the spine. Cancer Control. 2007;14:405-11.
16. Bartels RH, van der Linden YM, van der Graaf WT. Spinal extradural metastasis: review of current treatment options. CA: a cancer journal for clinicians. 2008;58:245-59.
17. Wilson BC, Patterson MS. The physics, biophysics and technology of photodynamic therapy. Physics in medicine and biology. 2008;53:R61-109.
18. Celli JP, Spring BQ, Rizvi I, Evans CL, Samkoe KS, Verma S, et al. Imaging and photodynamic therapy: mechanisms, monitoring, and optimization. Chem Rev. 2010;110:2795-838.

19. Pervaiz S, Olivo M. Art and science of photodynamic therapy. Clin Exp Pharmacol Physiol. 2006;33:551-6.
20. Akens MK, Hardisty MR, Wilson BC, Schwock J, Whyne CM, Burch S, et al. Defining the therapeutic window of vertebral photodynamic therapy in a murine pre-clinical model of breast cancer metastasis using the photosensitizer BPD-MA (Verteporfin). Breast cancer research and treatment. 2010;119:325-33.
21. Akens MK, Yee AJ, Wilson BC, Burch S, Johnson CL, Lilge L, et al. Photodynamic therapy of vertebral metastases: evaluating tumor-to-neural tissue uptake of BPD-MA and ALA-PpIX in a murine model of metastatic human breast carcinoma. Photochem Photobiol. 2007;83:1034-9.
22. Burch S, Bisland SK, Bogaards A, Yee AJ, Whyne CM, Finkelstein JA, et al. Photodynamic therapy for the treatment of vertebral metastases in a rat model of human breast carcinoma. J Orthop Res. 2005;23:995-1003.
23. Burch S, Bogaards A, Siewerdsen J, Moseley D, Yee A, Finkelstein J, et al. Photodynamic therapy for the treatment of metastatic lesions in bone: studies in rat and porcine models. J Biomed Opt. 2005;10:034011.
24. Won E, Akens MK, Hardisty MR, Burch S, Bisland SK, Yee AJ, et al. Effects of photodynamic therapy on the structural integrity of vertebral bone. Spine. 2010;35:272-7.
25. Won E, Wise-Milestone L, Akens MK, Burch S, Yee AJ, Wilson BC, et al. Beyond bisphosphonates: photodynamic therapy structurally augments metastatically involved vertebrae and destroys tumor tissue. Breast cancer research and treatment. 2010.
26. Zheng G, Chen J, Stefflova K, Jarvi M, Li H, Wilson BC. Photodynamic molecular beacon as an activatable photosensitizer based on protease-controlled singlet oxygen quenching and activation. Proceedings of the National Academy of Sciences of the United States of America. 2007;104:8989-94.
27. Lo PC, Chen J, Stefflova K, Warren MS, Navab R, Bandarchi B, et al. Photodynamic molecular beacon triggered by fibroblast activation protein on cancer-associated fibroblasts for diagnosis and treatment of epithelial cancers. J Med Chem. 2009;52:358-68.
28. Bogaards A, Varma A, Zhang K, Zach D, Bisland SK, Moriyama EH, et al. Fluorescence image-guided brain tumour resection with adjuvant metronomic photodynamic therapy: pre-clinical model and technology development. Photochem Photobiol Sci. 2005;4:438-42.
29. Troyan SL, Kianzad V, Gibbs-Strauss SL, Gioux S, Matsui A, Oketokoun R, et al. The FLARE intraoperative near-infrared fluorescence imaging system: a first-in-human clinical trial in breast cancer sentinel lymph node mapping. Ann Surg Oncol. 2009;16:2943-52.
30. Stenzl A, Burger M, Fradet Y, Mynderse LA, Soloway MS, Witjes JA, et al. Hexaminolevulinate guided fluorescence cystoscopy reduces recurrence in patients with nonmuscle invasive bladder cancer. J Urol. 2010;184:1907-13.
31. Upile T, Jerjes W, Sterenborg HJ, El-Naggar AK, Sandison A, Witjes MJ, et al. Head & neck optical diagnostics: vision of the future of surgery. Head Neck Oncol. 2009;1:25.
32. Wilson BC. Detection and treatment of dysplasia in Barrett's esophagus: a pivotal challenge in translating biophotonics from bench to bedside. J Biomed Opt. 2007;12:051401.

33. Gibbs-Strauss SL, O'Hara JA, Hoopes PJ, Hasan T, Pogue BW. Noninvasive measurement of aminolevulinic acid-induced protoporphyrin IX fluorescence allowing detection of murine glioma in vivo. J Biomed Opt. 2009;14:014007.
34. Jiang T, Olson ES, Nguyen QT, Roy M, Jennings PA, Tsien RY. Tumor imaging by means of proteolytic activation of cell-penetrating peptides. Proceedings of the National Academy of Sciences of the United States of America. 2004;101:17867-72.
35. McIntyre JO, Fingleton B, Wells KS, Piston DW, Lynch CC, Gautam S, et al. Development of a novel fluorogenic proteolytic beacon for in vivo detection and imaging of tumour-associated matrix metalloproteinase-7 activity. Biochem J. 2004;377:617-28.
36. Weissleder R, Ntziachristos V. Shedding light onto live molecular targets. Nat Med. 2003;9:123-8.
37. Weissleder R, Tung CH, Mahmood U, Bogdanov A, Jr. In vivo imaging of tumors with protease-activated near-infrared fluorescent probes. Nat Biotechnol. 1999;17:375-8.
38. Lee S, Xie J, Chen X. Activatable molecular probes for cancer imaging. Curr Top Med Chem. 2010;10:1135-44.
39. Muller PJ, Wilson BC. Photodynamic therapy of brain tumors--a work in progress. Lasers Surg Med. 2006;38:384-9.

Figure 1A. MMP involvement in the tumor-bone vicious cycle.

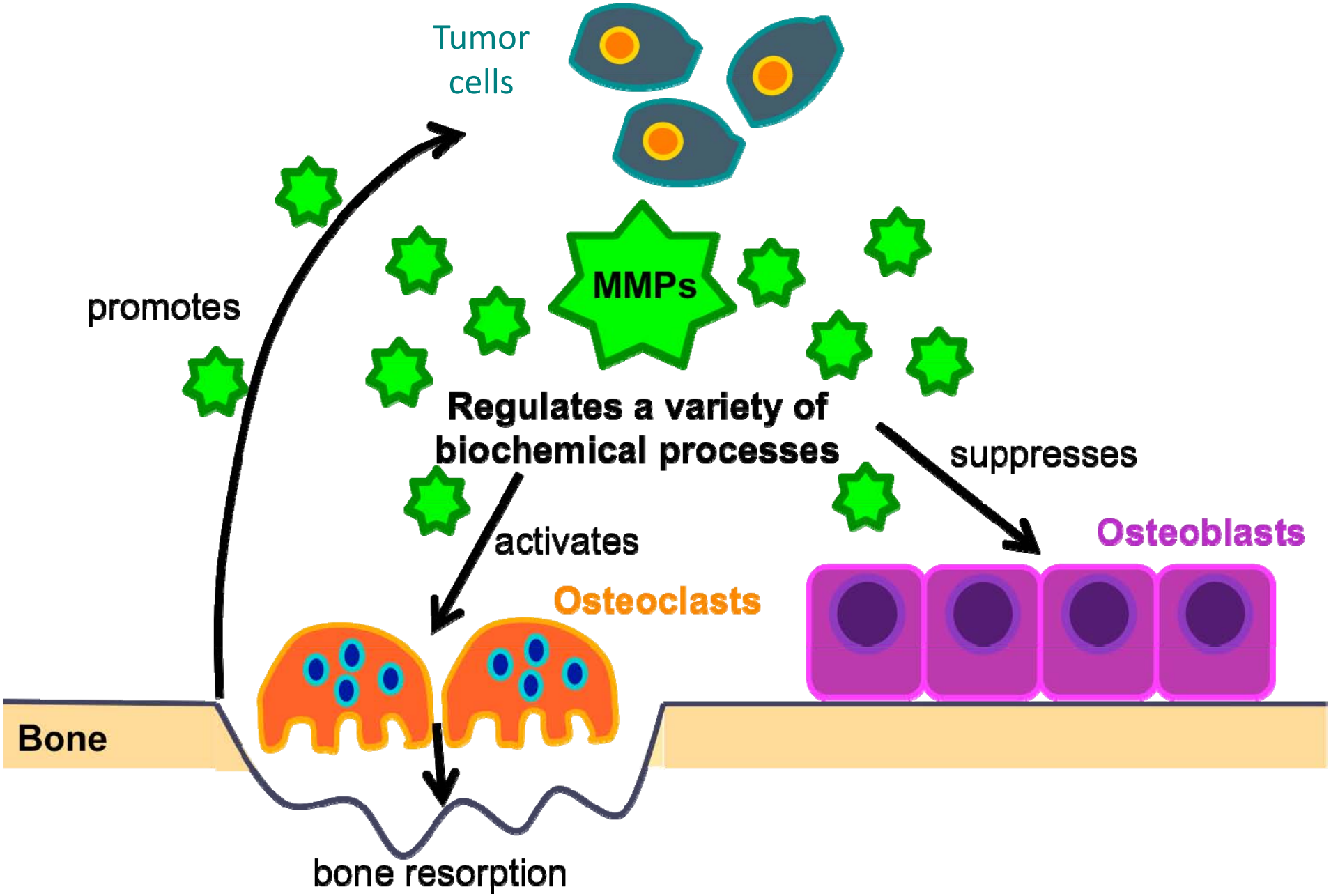

Figure 1B. Schematic of photodynamic molecular beacon ($PP_{MMP}B$) activation. A) the beacon accumulates in tissue but remains photodynamically and optically silent (A) until cleaved by MMPs at sites of vertebral metastases (B), which restores both its fluorescence for imaging and generation of singlet oxygen for treatment (C).

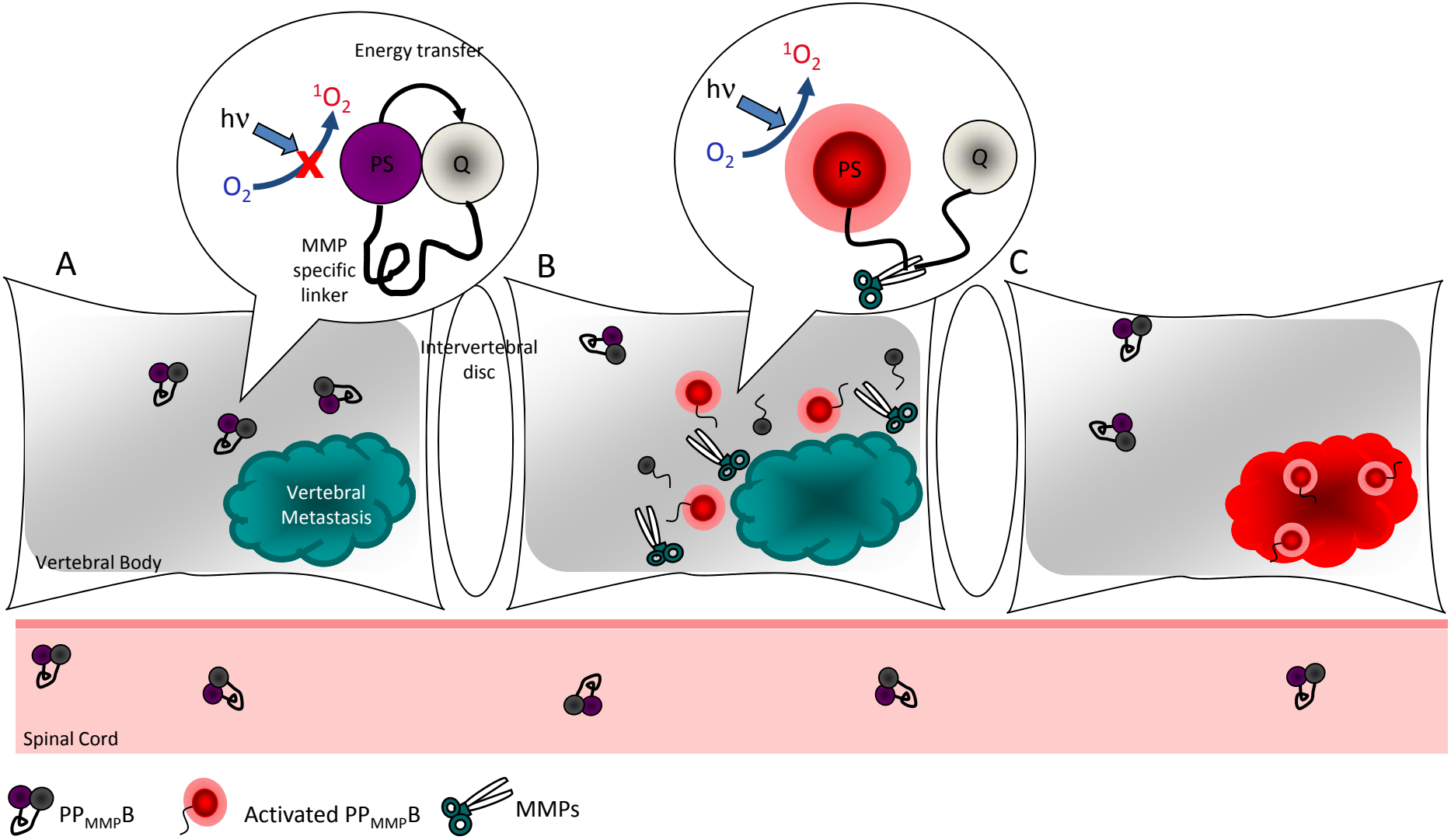

Figure 2. *In vivo* breast cancer vertebral metastases model. A) Bioluminescent imaging of MT-1 at 14 days after intracardiac injection of 1x10^{6}cells, showing multiple sites of metastitic growth, including in the spine.. B) Example of immunohistology section of vertebral column where hEGFr immunhisto stains for viable tumor (T- tumor, SC - spinal cord, IVD - intervertebral disc, L - lumbar, Th - thoracic)

A

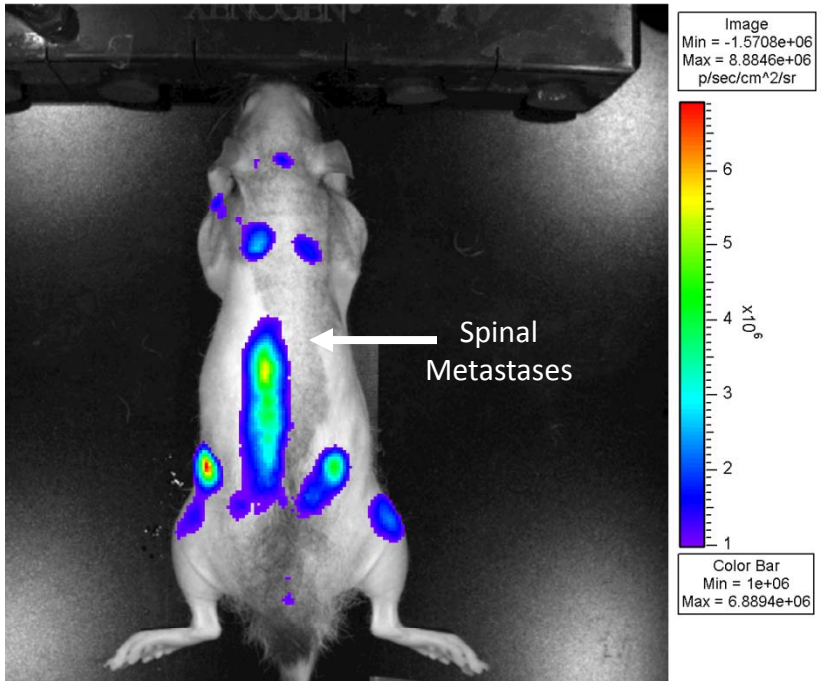

B

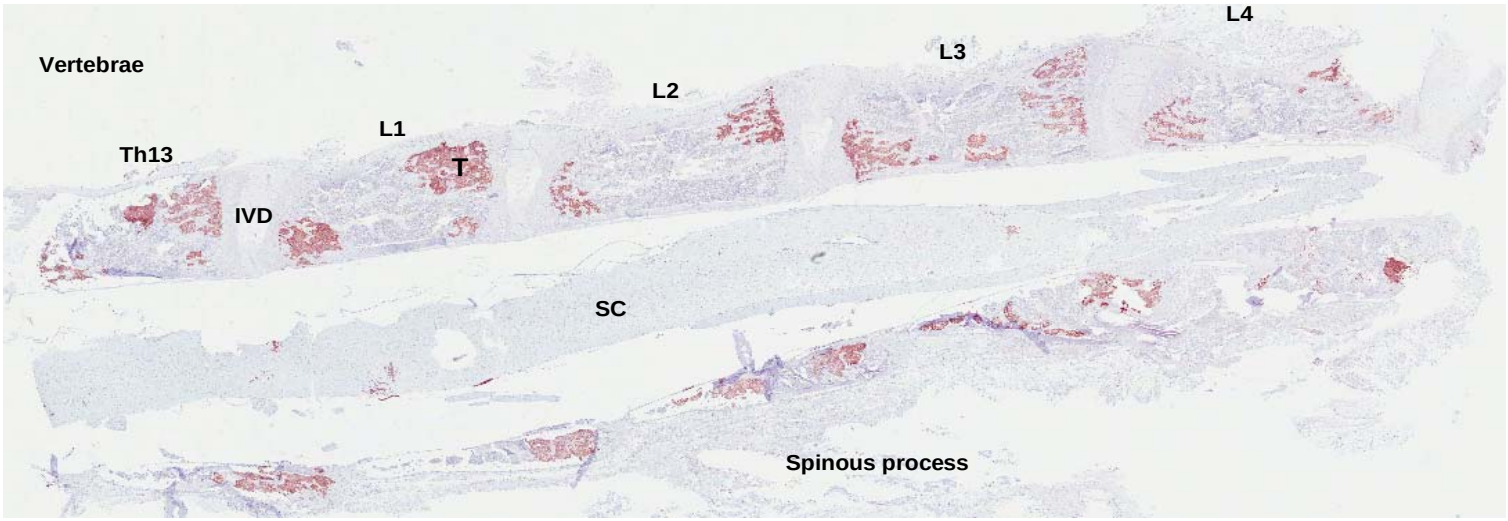

Figure 3. *In vitro* fluorescence and corresponding brightfield images of MT-1 cells after 6h incubation in beacon: A) 10uM $PP_{MMP}B$, B) 10uM $PP_{scrambled}B$. C) Flow cytometry after 1 and 3 h incubation (n=3 samples)

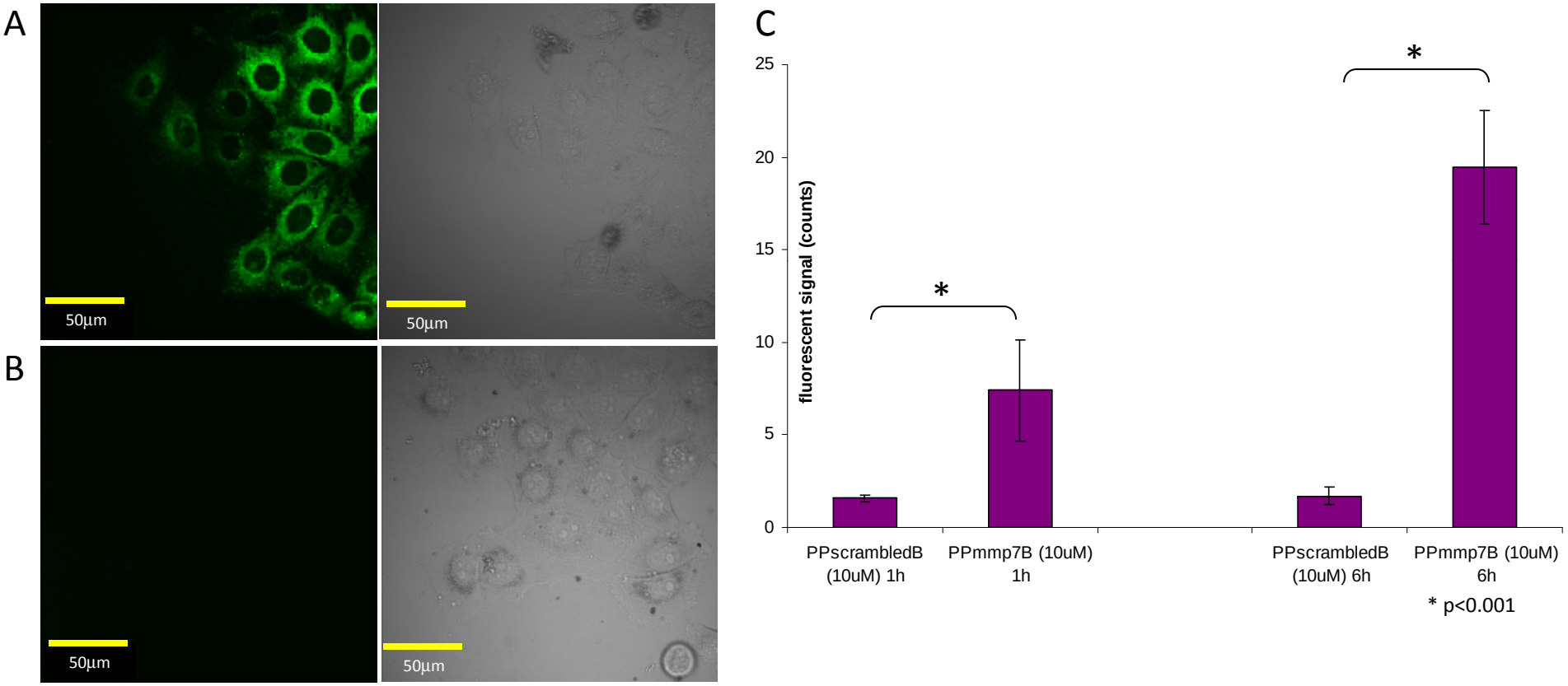

Figure 4. *In vivo* fluorescence images in the MT-1 subcutaneous xenogfart tumor model. A) before (i) and 17 h after (ii) i.v. injection of 2 mg/kg $PP_{MMP}B$, B) corresponding $PP_{scrambled}B$ images at (i) 10 min, (ii) 6h and (iii) 24h post injection. C) Fluorescence micrographs and corresponding differential contrast images of $PP_{MMP}B$ in MT-1 frozen tissue sections, and D) corresponding $PP_{scrambled}B$ images (n=5)

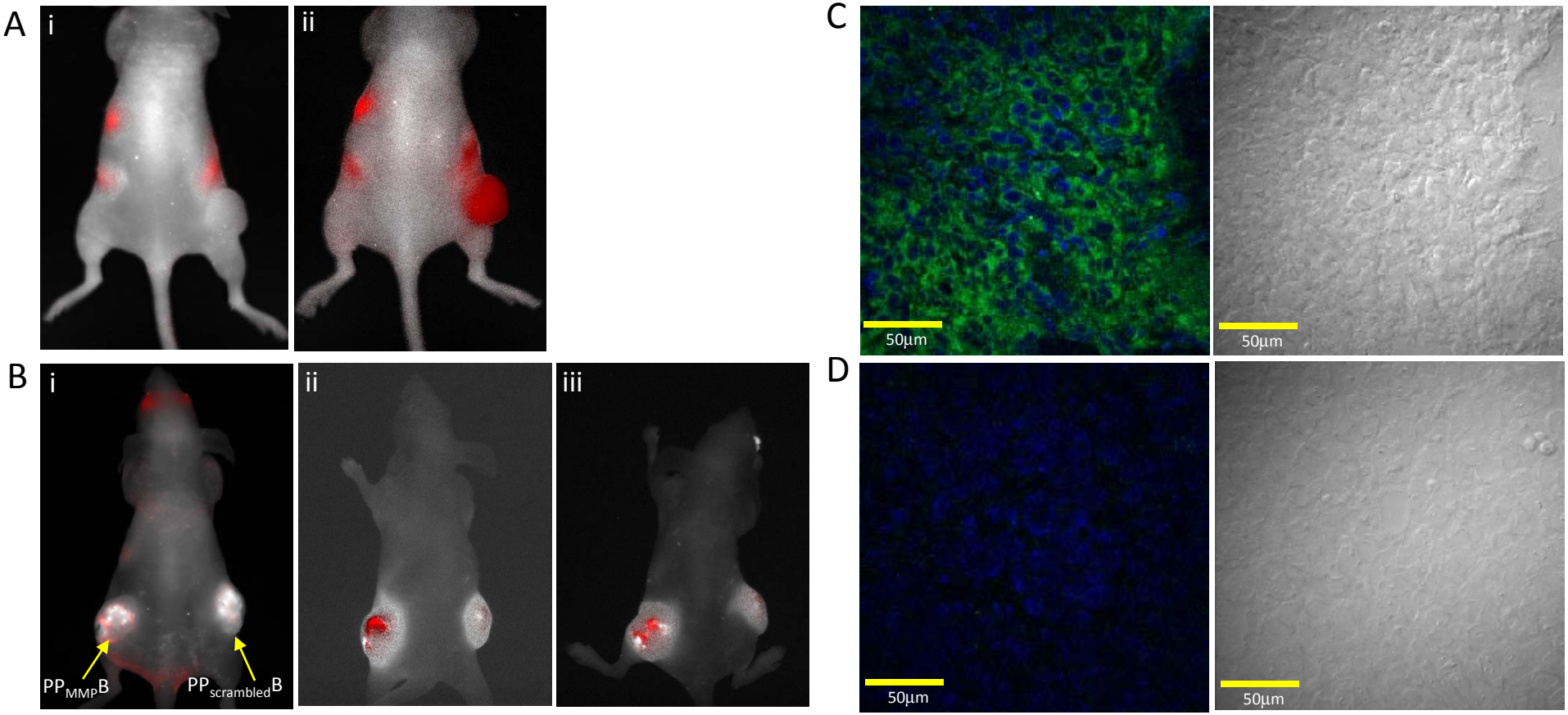

Figure 5 Time-dependent activation of $PP_{MMP}B$ by vertebral metastases imagesd *ex vivo*. A) Composite fluorescence images at 2, 4, 12 and 24h after intravenous injection of 3 mg/kg $PP_{MMP}B$: SC – spinal cord, VB – vertebral body, IVD – intervertebral disc. B) Average fluorescent signal comparing the vertebrae and spinal cord: * indicates statically significant difference between 2h versus 12h and 24h time points in $PP_{MMP}B$ activation in the vertebrae (n=4 for 2 and 4h time points, n=2 for 12 and 24h).

A

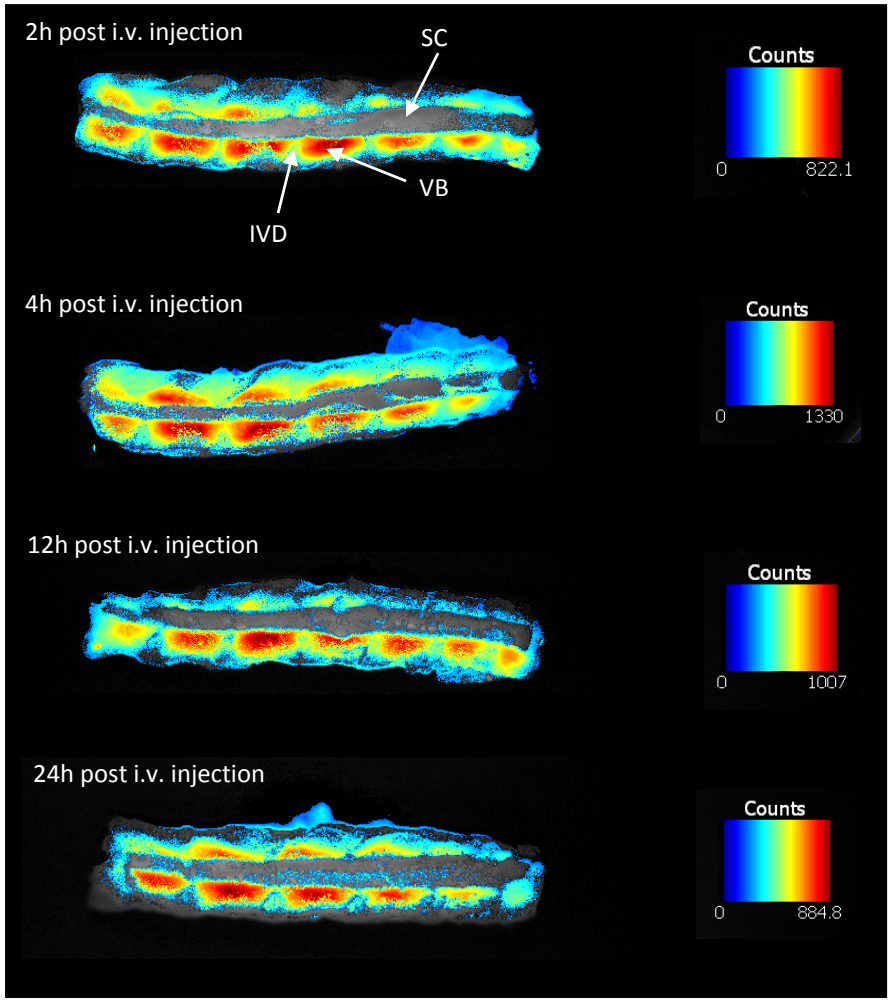

B

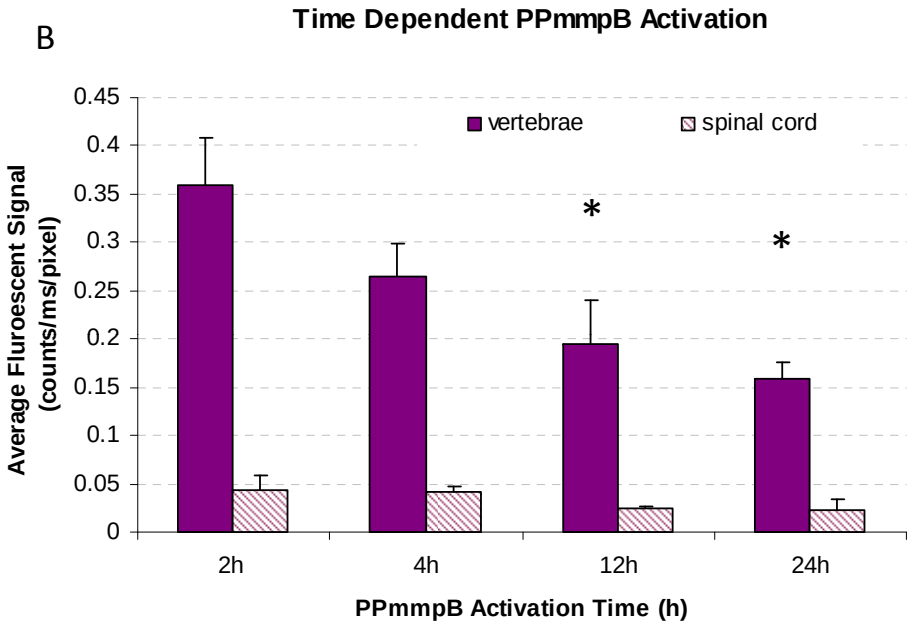

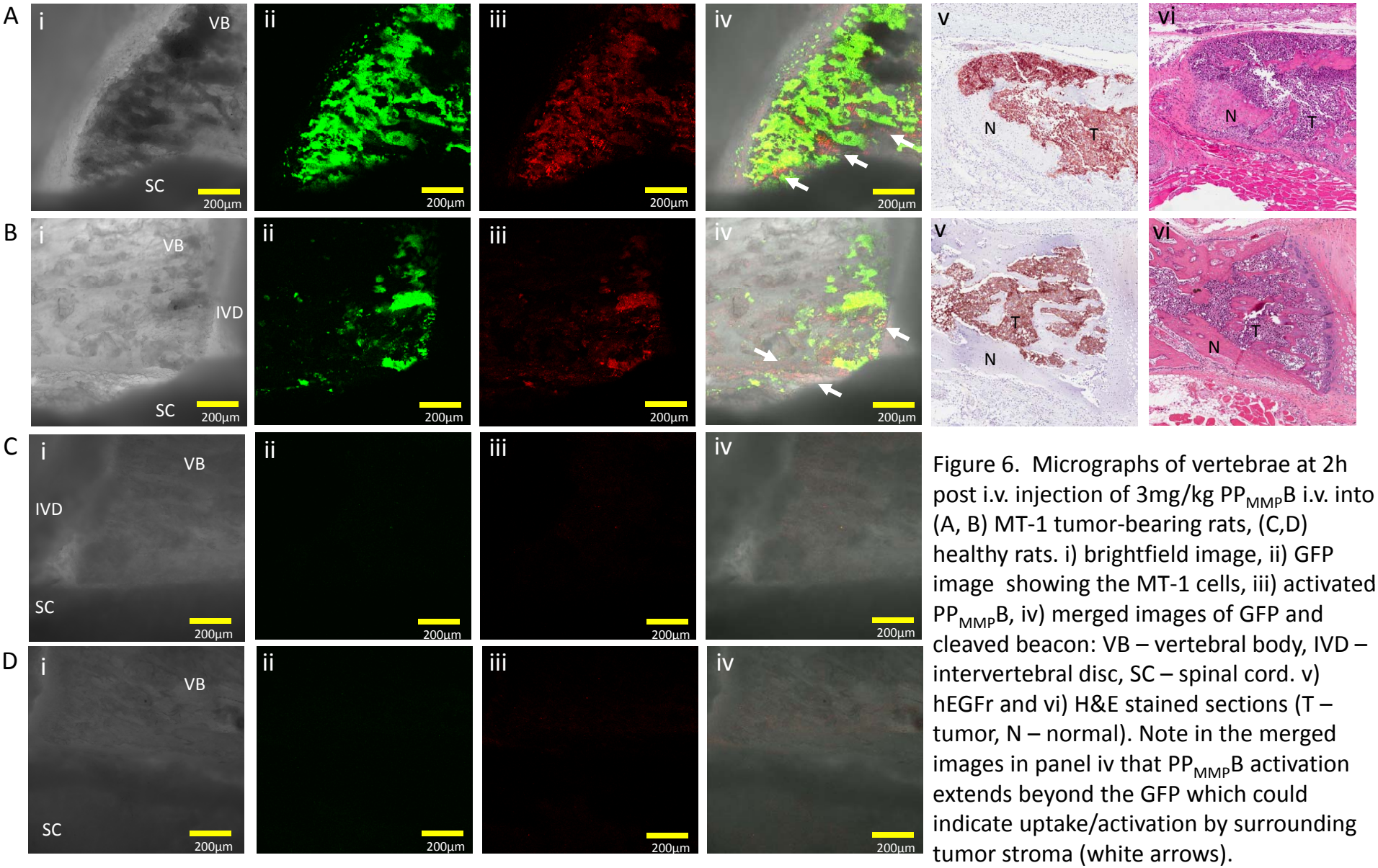

Figure 6. Micrographs of vertebrae at 2h post i.v. injection of 3mg/kg $PP_{MMP}B$ i.v. into (A, B) MT-1 tumor-bearing rats, (C,D) healthy rats. i) brightfield image, ii) GFP image showing the MT-1 cells, iii) activated $PP_{MMP}B$, iv) merged images of GFP and cleaved beacon: VB – vertebral body, IVD – intervertebral disc, SC – spinal cord. v) hEGFr and vi) H&E stained sections (T – tumor, N – normal). Note in the merged images in panel iv that $PP_{MMP}B$ activation extends beyond the GFP which could indicate uptake/activation by surrounding tumor stroma (white arrows).